TECHNICAL REPORT ARMID-TR-78001

DESIGN CHARTS FOR TORSIONAL PROPERTIES OF NON-CIRCULAR SHAFTS

ROBERT I. ISAKOWER

NOVEMBER 1978

US ARMY ARMAMENT RESEARCH AND DEVELOPMENT COMMAND
MANAGEMENT INFORMATION
SYSTEMS DIRECTORATE
DOVER, NEW JERSEY

UNCLASSIFIED

SECURITY CLASSIFICATION OF THIS PAGE *(When Data Entered)*

REPORT DOCUMENTATION PAGE

READ INSTRUCTIONS BEFORE COMPLETING FORM

1. REPORT NUMBER: Technical Report ARMID-TR-78001
2. GOVT ACCESSION NO.:
3. RECIPIENT'S CATALOG NUMBER:

4. TITLE *(and Subtitle)*: DESIGN CHARTS FOR TORSIONAL PROPERTIES OF NON-CIRCULAR SHAFTS

5. TYPE OF REPORT & PERIOD COVERED: Final

6. PERFORMING ORG. REPORT NUMBER:

7. AUTHOR(s): Robert I. Isakower

8. CONTRACT OR GRANT NUMBER(s):

9. PERFORMING ORGANIZATION NAME AND ADDRESS:
ARRADCOM, MISD
ATTN: DRDAR-MSA
Dover, NJ 07801

10. PROGRAM ELEMENT, PROJECT, TASK AREA & WORK UNIT NUMBERS:

11. CONTROLLING OFFICE NAME AND ADDRESS:
ARRADCOM, TSD
ATTN: DRDAR-TSS
Dover, NJ 07801

12. REPORT DATE: November 1978

13. NUMBER OF PAGES: 90

14. MONITORING AGENCY NAME & ADDRESS *(if different from Controlling Office)*:
ARRADCOM, MISD
ATTN: DRDAR-MSA
Dover, NJ 07801

15. SECURITY CLASS. *(of this report)*: Unclassified

15a. DECLASSIFICATION/DOWNGRADING SCHEDULE:

16. DISTRIBUTION STATEMENT *(of this Report)*

Approved for public release; distribution unlimited.

17. DISTRIBUTION STATEMENT *(of the abstract entered in Block 20, if different from Report)*

18. SUPPLEMENTARY NOTES

19. KEY WORDS *(Continue on reverse side if necessary and identify by block number)*

Torsion	Membrane	Finite
Shafts	Poisson	Differences
Torque	Soap-film	
Stress	Prandtl	

20. ABSTRACT *(Continue on reverse side if necessary and identify by block number)*

Design charts and tables have been developed for the elastic torsional stress analyses of prismatic shafts, splines, and spring bars with virtually all commonly encountered cross sections. Circular shafts with rectangular and circular key-ways, external splines, and milled flats along with rectangular and X-shaped torsion bars are presented. A computer program was developed at the U.S. Army ARRADCOM, Dover, NJ site, which provides a finite difference solution to the

DD FORM 1 JAN 73 1473 EDITION OF 1 NOV 65 IS OBSOLETE

UNCLASSIFIED

SECURITY CLASSIFICATION OF THIS PAGE *(When Data Entered)*

20. ABSTRACT (Continued)

governing partial differential equation (Poisson's) which defines the stress function. Using the stress function solution for the various shapes and Prandtl's membrane analogy, the author is able to produce dimensionless design charts for transmitted torque and maximum shearing stress. Additionally, the transmitted torque (or twisting moment) of hollow shafts can be obtained by using the principles of parallel shafts, even if both inner and outer cross-sectional contours are non-circular and of different shapes.

ACKNOWLEDGMENTS

The author would like to thank the following people for their assistance in the preparation of this report:

Mr. Robert E. Barnas, MISD, ARRADCOM, for programming the CLYDE solution.

SP4 Lillian Ishibashi, Cardiovascular Lab, Ft. Sam Houston, Texas, for preparing the input data program.

Mr. Joseph J. Sierodzinski, MISD, ARRADCOM, for the photography.

TABLE OF CONTENTS

Tables

Figures

THE TORSION PROBLEM

The elastic stress analysis of uniformly circular shafts in torsion is a familiar and straightforward concept to design engineers. As the bar is twisted, plane sections remain plane, radii remain straight, and each section rotates about the longitudinal axis. The shear stress at any point is proportional to the distance from the center, and the stress vector lies in the plane of the circular section and is perpendicular to the radius to the point, with the maximum stress tangent to the outer face of the bar. (Another shearing stress of equal magnitude acts at the same point in the longitudinal direction.) The torsional stiffness is a function of material property, angle of twist, and the polar moment of inertia of the circular cross-section. These relationships are expressed as:

$$\theta = T/J \cdot G, \text{ or } T = G \cdot \theta \cdot J$$

and $$S_s = T \cdot r/J, \text{ or } S_s = G \cdot \theta \cdot r$$

where T = twisting moment or transmitted torque, G = Modulus of Rigidity of the shaft material, θ = angle of twist per unit length of the shaft, J = polar moment of inertia of the (circular) cross-section, S_s = shear stress, and r = radius to any point.

However, if the cross-section of the bar deviates even slightly from a circle, the situation changes radically and far more complex design equations are required. Sections of the bar do not remain plane, but warp into surfaces, and radial lines through the center do not remain straight. The distribution of shear stress on the section is no longer linear, and the direction of shear stress is not normal to a radius.

The governing equation of continuity (or compatibility) from Saint-Venant's theory is

$$\frac{\partial^2 \varphi}{\partial X^2} + \frac{\partial^2 \varphi}{\partial Y^2} = -2G\theta$$

where Φ = Saint-Venant's torsion stress function. The problem then is to find a Φ function which satisfies this equation and also the boundary conditions that Φ = a constant along the boundary. This Φ function has the nature of a potential function, such as voltage, hydrodynamic velocity, or gravitational height. Its absolute value is, therefore, not important; only relative values or differences are meaningful.

The solutions to this equation required complicated mathematics. Even simple, but commonplace, practical cross-sections could not be easily reduced to manageable mathematical formulae, and numerical approximations or intuitive methods had to be used.

One of the most effective numerical methods to solve for Saint-Venant's torsion stress function is that of finite differences. The CLYDE computer program was applied to a number of shafts to produce the dimensionless design charts on the following pages. Most of the charts required approximately 50 computer runs for plot data generation, but once completed, the design charts for that cross-section are good for virtually all combinations of dimensions, material, and shaft twist.

The three-dimensional plot of Φ over the cross-section is a surface and, with Φ set to zero (a valid constant) along the periphery, the surface is a domb or Φ membrane.[1] The transmitted torque (T) is proportional to twice the volume under the membrane and the stress (S_s) is proportional to the slope of the membrane in the direction perpendicular to the measured slope. Neglecting the stress concentration of sharp re-entrant corners, which are relieved with generous fillets, the maximum stress for bars with solid cross sections is at the point on the periphery nearest the center (fig. 1).

[1]The best intuitive method, the membrane analogy, came from Prandtl. He showed that the compatibility equation for a twisted bar was the "same" as the equation for a membrane stretched over a hole in a flat plate, then inflated. This concept provides a simple way to visualize the torsional stress characteristics of shafts of any cross-section relative to those of circular shafts for which an exact analytical solution is readily obtainable.

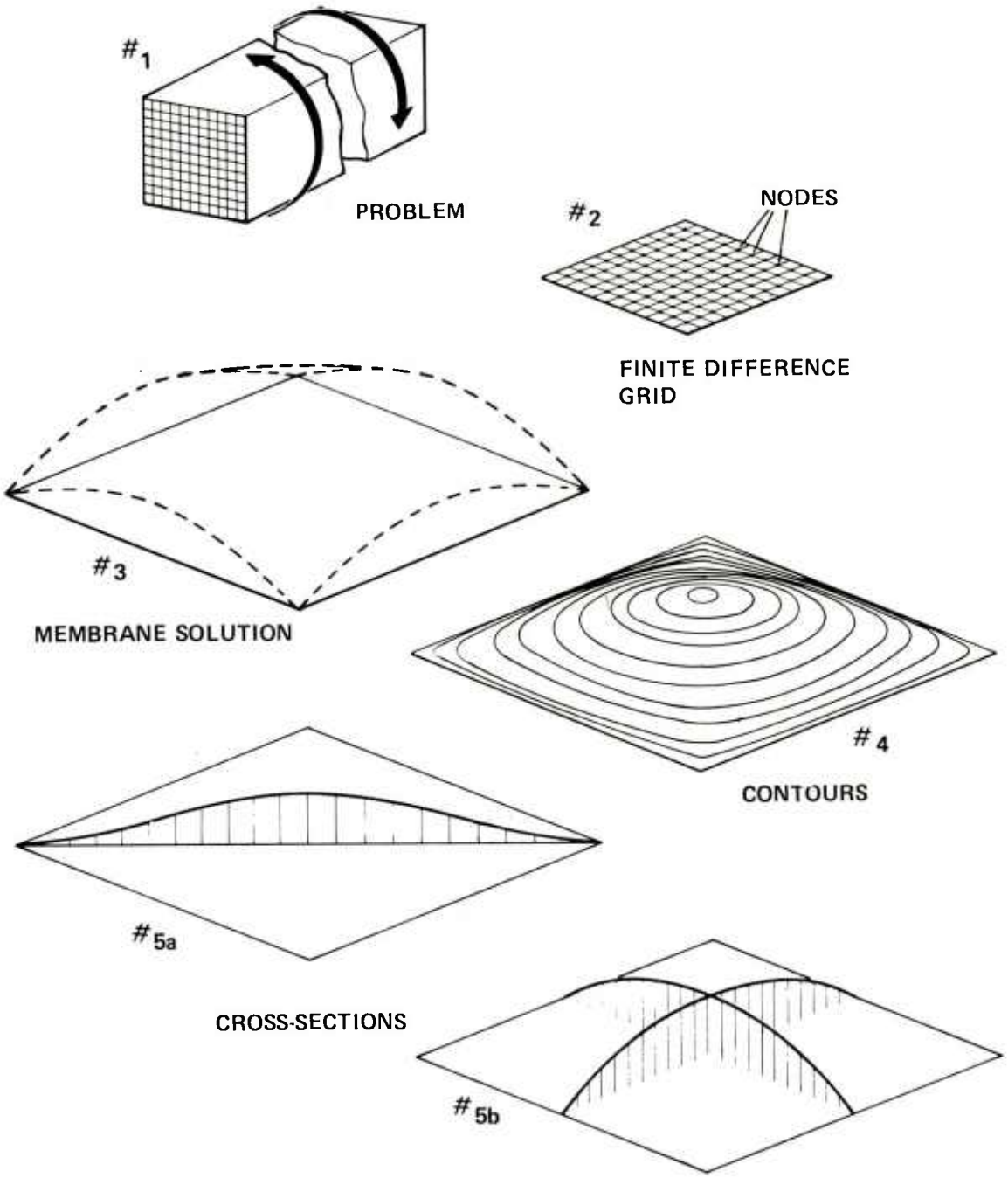

Figure 1. Membrane analogy.

DESIGN CHARTS AND TABLES

Design charts and related data which support the elastic torsional stress analyses conducted by MISD are shown in figures 2 through 25 and tables 2 through 25, respectively. The item nomenclature used in the analyses is given in table 1.

These data are based on the stress function solution for various shapes provided by the CLYDE computer program and on Prandtl's membrane analogy.

Since the design charts are dimensionless, they can be used for shafts of any material and any dimensions.

Table 1. Element nomenclature

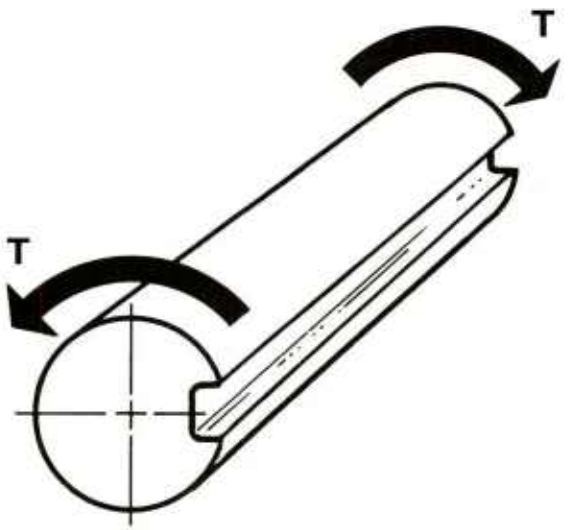

T = TRANSMITTED TORQUE, N - m (lb - in.)

θ = ANGLE OF TWIST PER UNIT LENGTH, rad/mm (rad/in.)

G = MODULUS OF RIGIDITY OR MODULUS OF ELASTICITY IN SHEAR, kPa (psi)

R = OUTER RADIUS OF CROSS-SECTION, mm (in.)

$V, \frac{d\phi}{ds}$ = VARIABLES FROM CHARTS (OR TABLES) RELATED TO VOLUME UNDER "SOAP FILM MEMBRANE" AND SLOPE OF "MEMBRANE"

S_s = SHEAR STRESS, kPa (psi)

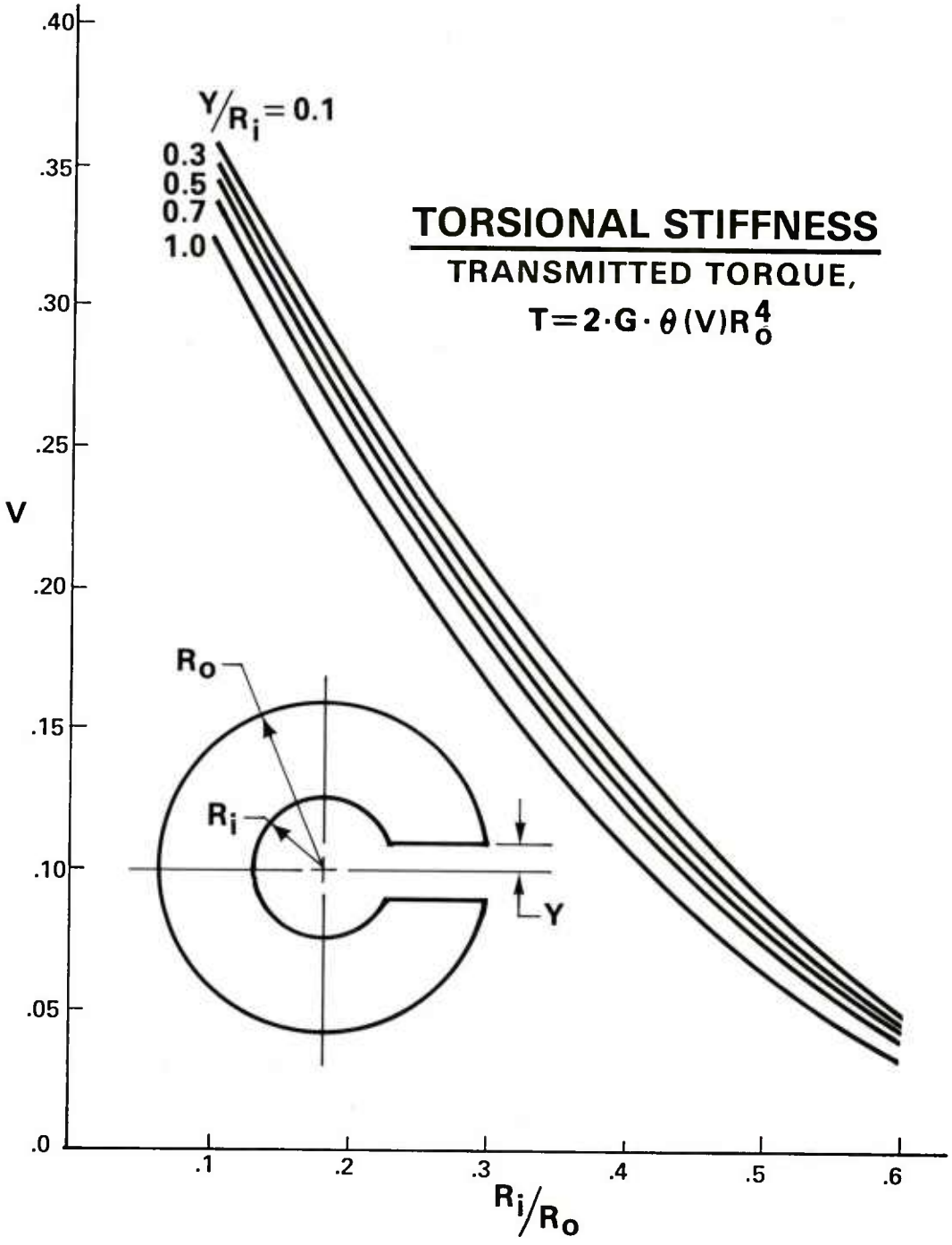

Figure 2. Split shaft, torque.

Table 2. Split shaft, volume factor (V)

Y/Ri	Ri/Ro					
	0.1	0.2	0.3	0.4	0.5	0.6
0.1	.3589	.2802	.2068	.1422	.0891	.0491
0.2	.3557	.2762	.2030	.1391	.0870	.0478
0.3	.3525	.2722	.1991	.1360	.0848	.0464
0.4	.3492	.2680	.1952	.1328	.0825	.0450
0.5	.3457	.2637	.1911	.1294	.0801	.0436
0.6	.3423	.2593	.1869	.1260	.0777	.0421
0.7	.3387	.2548	.1824	.1223	.0750	.0405
0.8	.3350	.2499	.1776	.1183	.0722	.0387
0.9	.3312	.2447	.1725	.1139	.0689	.0367
1.0	.3269	.2389	.1665	.1087	.0649	.0340

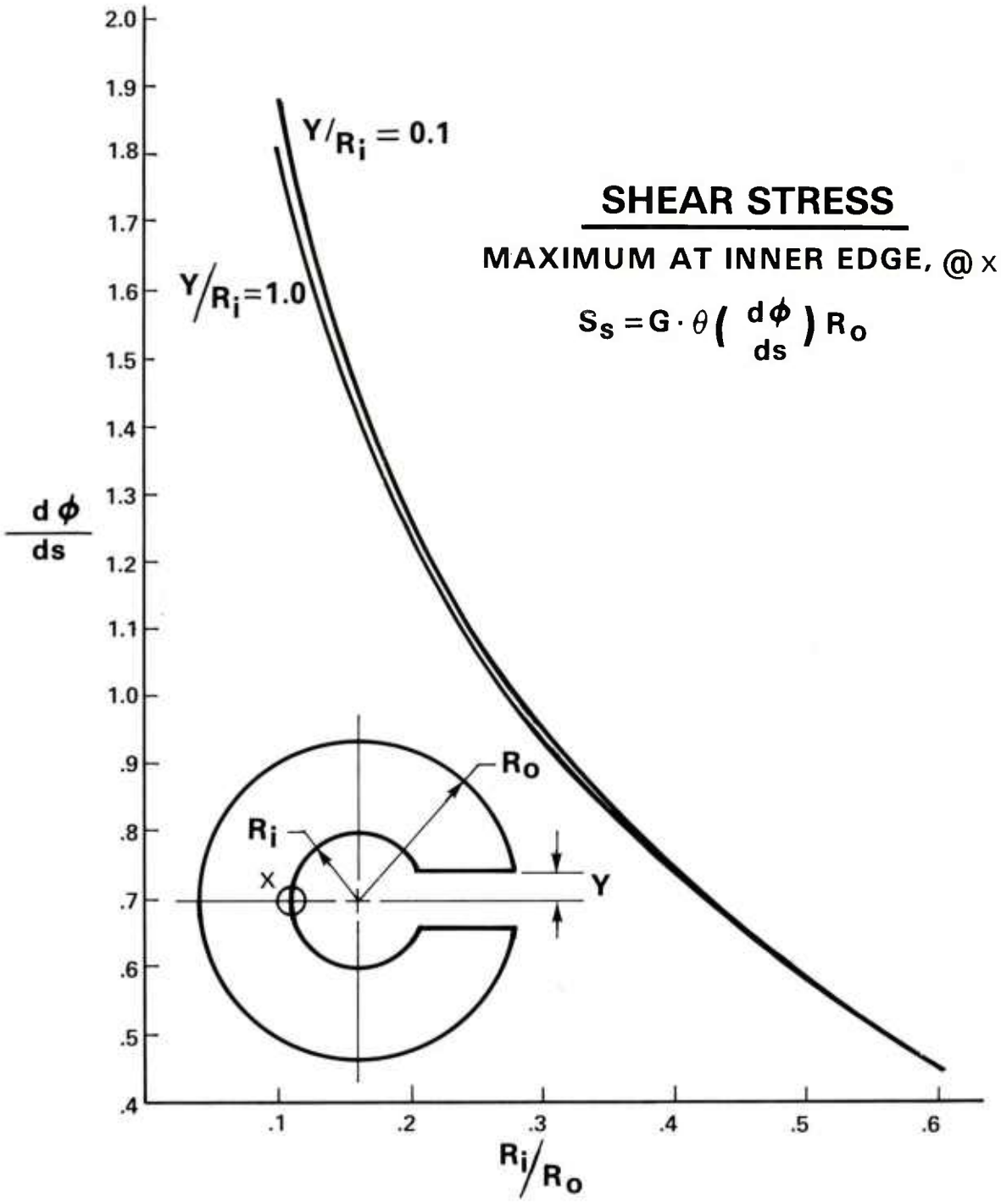

Figure 3. Split shaft, stress.

Table 3. Split shaft, slope factor ($d\Phi/ds$)

Y/Ri	Ri/Ro					
	0.1	0.2	0.3	0.4	0.5	0.6
0.1	1.8987	1.2663	.9520	.7384	.5773	.4405
0.2	1.8953	1.2656	.9519	.7384	.5773	.4405
0.3	1.8916	1.2648	.9518	.7384	.5773	.4405
0.4	1.8875	1.2639	.9517	.7384	.5773	.4405
0.5	1.8829	1.2629	.9515	.7384	.5773	.4405
0.6	1.8778	1.2617	.9512	.7383	.5773	.4405
0.7	1.8722	1.2603	.9509	.7383	.5773	.4405
0.8	1.8661	1.2585	.9505	.7382	.5773	.4405
0.9	1.8585	1.2561	.9499	.7381	.5773	.4405
1.0	1.8484	1.2526	.9488	.7378	.5773	.4405

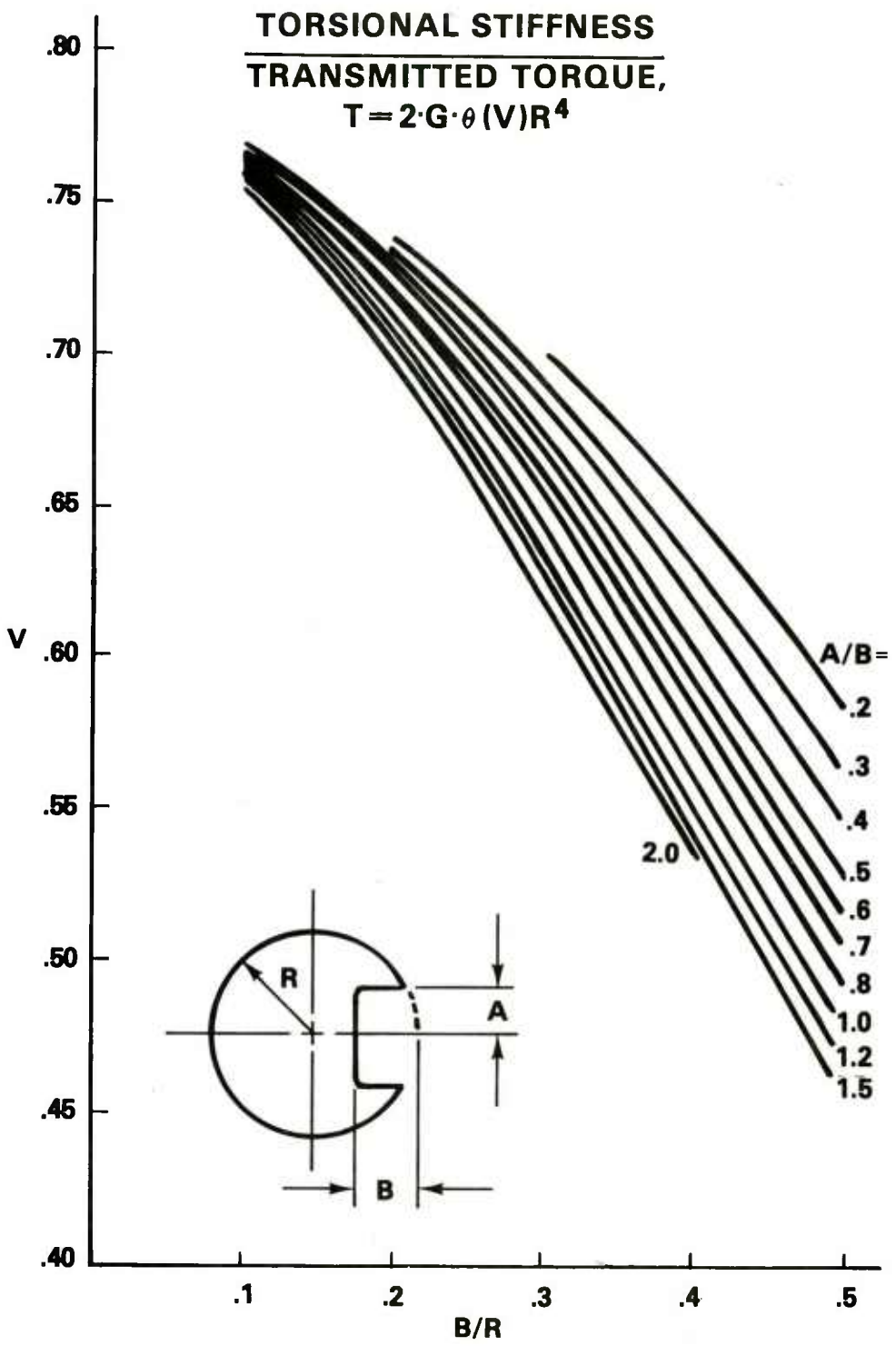

Figure 4. Single keyway shaft, torque.

Table 4. Single keyway shaft, volume factor (V)

A/B	B/R				
	0.1	0.2	0.3	0.4	0.5
0.2			.6994	.6472	.5864
0.3		.7379	.6900	.6316	.5648
0.4		.7341	.6816	.6173	.5459
0.5	.7682	.7290	.6725	.6043	.5294
0.6	.7676	.7262	.6663	.5941	.5152
0.7	.7668	.7224	.6592	.5848	.5032
0.8	.7658	.7190	.6533	.5762	.4931
0.9	.7647	.7162	.6480	.5686	.4849
1.0	.7633	.7125	.6424	.5619	.4783
1.2	.7621	.7079	.6347	.5531	.4697
1.5	.7592	.7012	.6260	.5449	.4649
2.0	.7560	.6945	.6200	.5424	

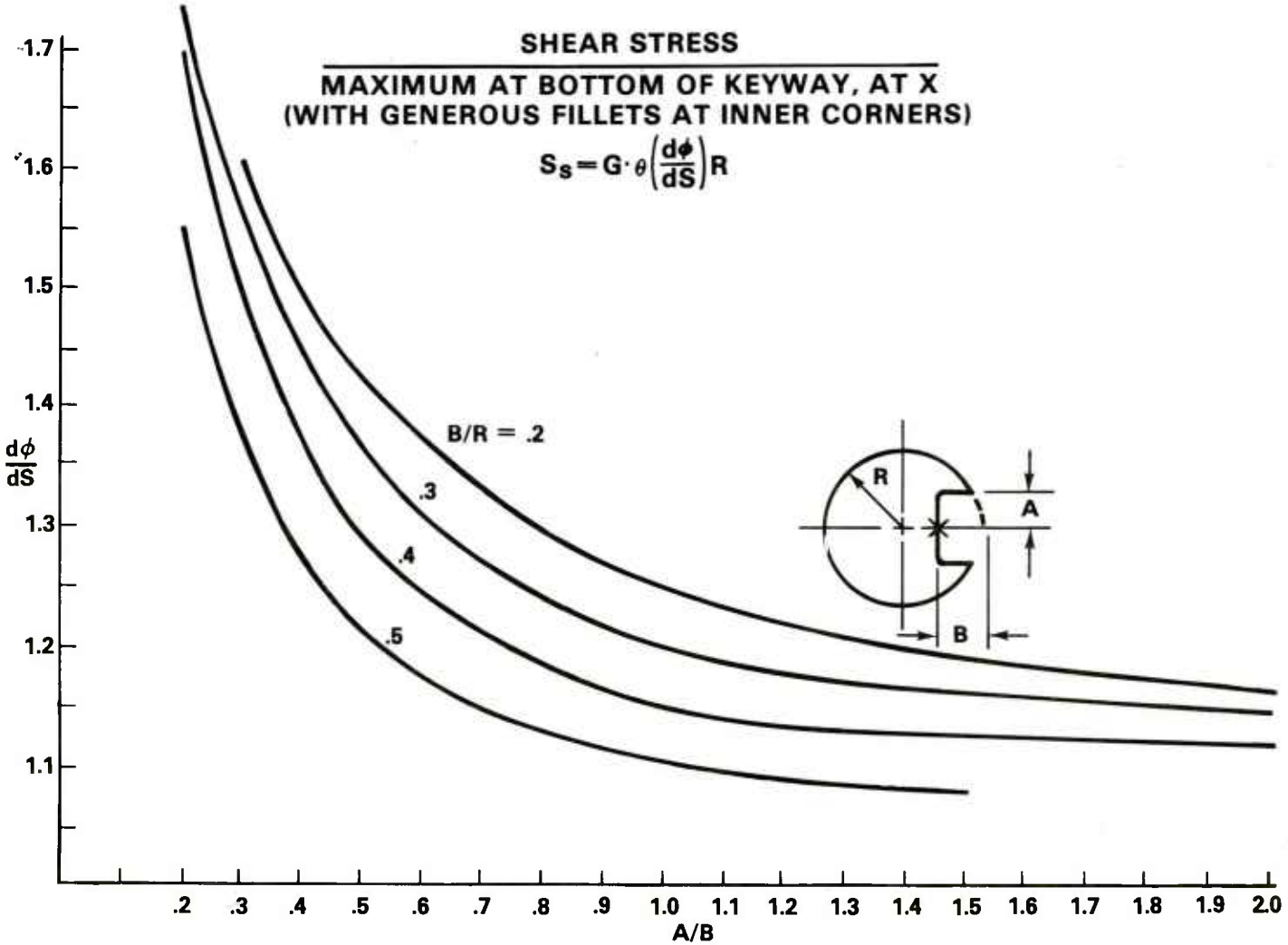

Figure 5. Single keyway shaft, stress.

Table 5. Single keyway shaft, slope factor ($d\Phi/ds$)

A/B	B/R				
	0.1	0.2	0.3	0.4	0.5
0.2			1.7316	1.6911	1.5473
0.3		1.6037	1.5729	1.4896	1.3753
0.4		1.5274	1.4565	1.3673	1.2750
0.5	1.4050	1.4158	1.3605	1.2888	1.2118
0.6	1.3890	1.3840	1.3213	1.2470	1.1702
0.7	1.3690	1.3383	1.2748	1.2128	1.1420
0.8	1.3438	1.2992	1.2465	1.1864	1.1226
0.9	1.3116	1.2783	1.2238	1.1669	1.1093
1.0	1.2698	1.2469	1.2022	1.1524	1.1002
1.2	1.2530	1.2215	1.1803	1.1374	1.0902
1.5	1.2057	1.1893	1.1605	1.1259	1.0858
2.0	1.1726	1.1680	1.1508	1.1234	

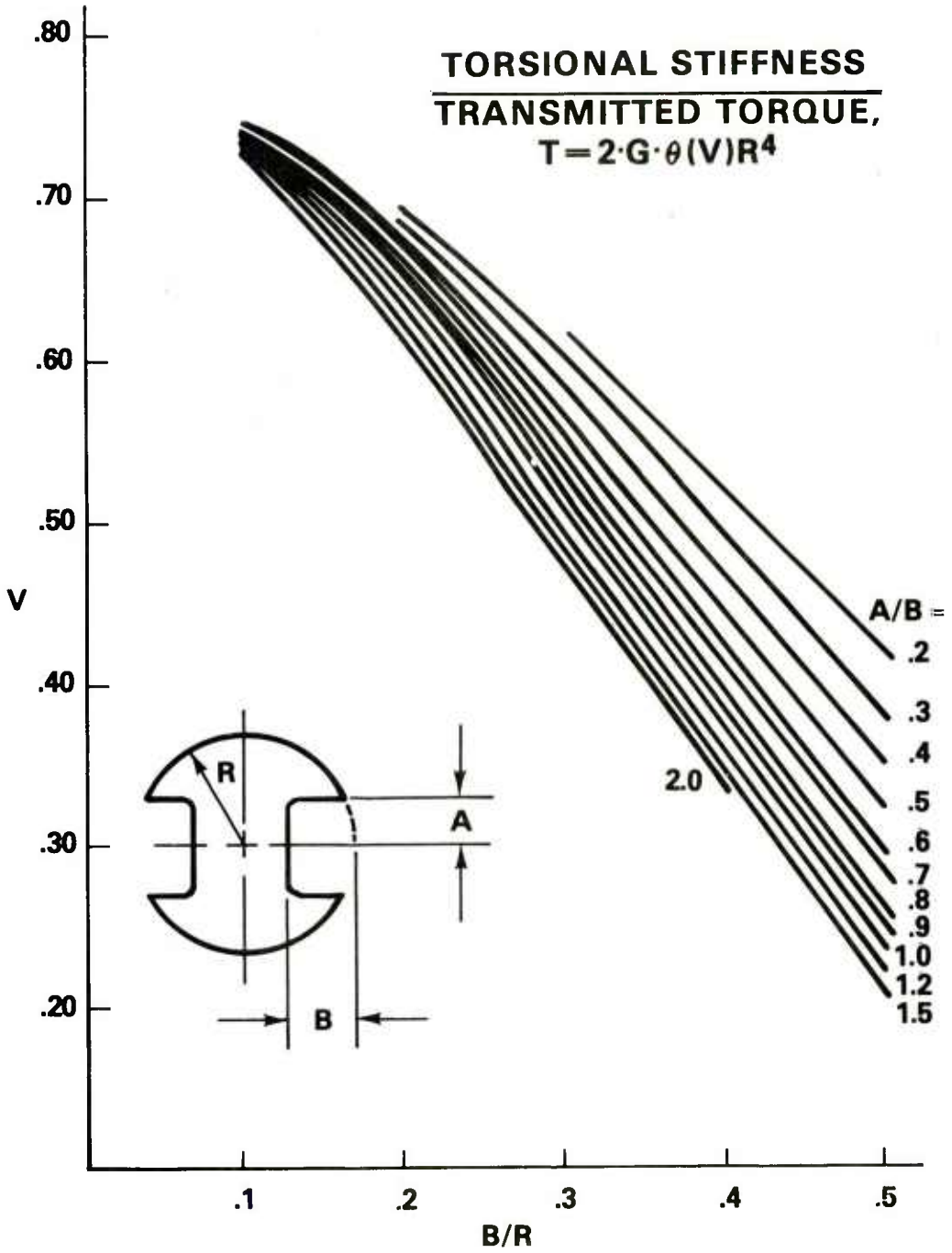

Figure 6. Two keyway shaft, torque.

Table 6. Two keyway shaft, volume factor (V)

A/B	B/R				
	0.1	0.2	0.3	0.4	0.5
0.2			.6187	.5226	.4195
0.3		.6927	.6008	.4944	.3831
0.4		.6853	.5848	.4688	.3517
0.5	.7524	.6753	.5678	.4457	.3246
0.6	.7511	.6698	.5562	.4277	.3014
0.7	.7496	.6625	.5429	.4112	.2818
0.8	.7477	.6558	.5319	.3962	.2655
0.9	.7454	.6505	.5221	.3829	.2522
1.0	.7426	.6433	.5117	.3713	.2416
1.2	.7404	.6344	.4974	.3559	.2276
1.5	.7346	.6215	.4813	.3416	.2197
2.0	.7283	.6086	.4703	.3373	

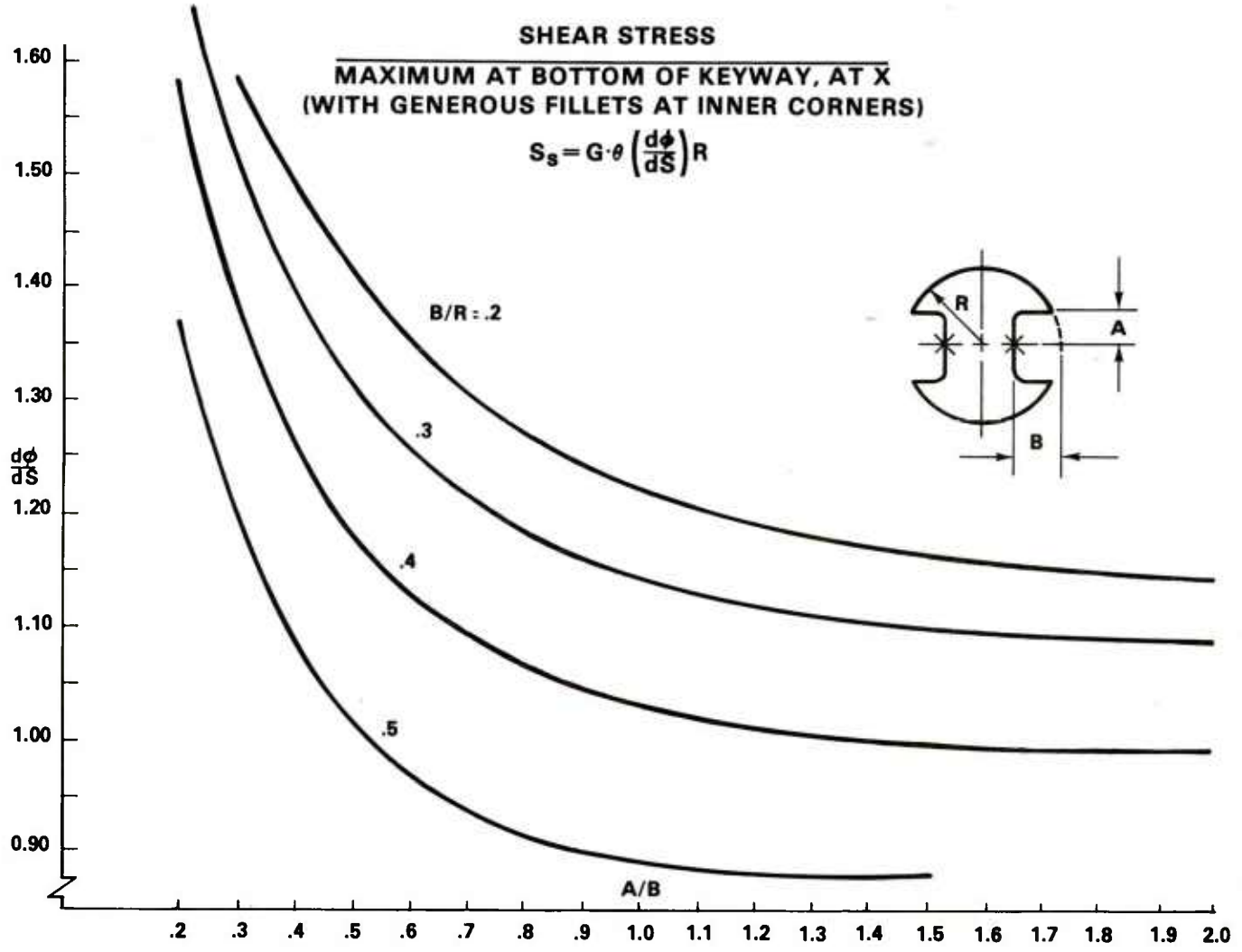

Figure 7. Two keyway shaft, stress.

Table 7. Two keyway shaft, slope factor ($d\Phi/ds$)

A/B	B/R				
	0.1	0.2	0.3	0.4	0.5
0.2			1.6802	1.5861	1.3645
0.3		1.5834	1.5203	1.3842	1.1911
0.4		1.5064	1.4028	1.2598	1.0872
0.5	1.4002	1.3939	1.3052	1.1785	1.0199
0.6	1.3840	1.3616	1.2645	1.1340	.9742
0.7	1.3639	1.3151	1.2163	1.0971	.9424
0.8	1.3385	1.2754	1.1865	1.0683	.9199
0.9	1.3061	1.2538	1.1624	1.0462	.9041
1.0	1.2641	1.2216	1.1392	1.0297	.8930
1.2	1.2470	1.1951	1.1151	1.0119	.8805
1.5	1.1991	1.1612	1.0927	.9978	.8749
2.0	1.1654	1.1382	1.0813	.9945	

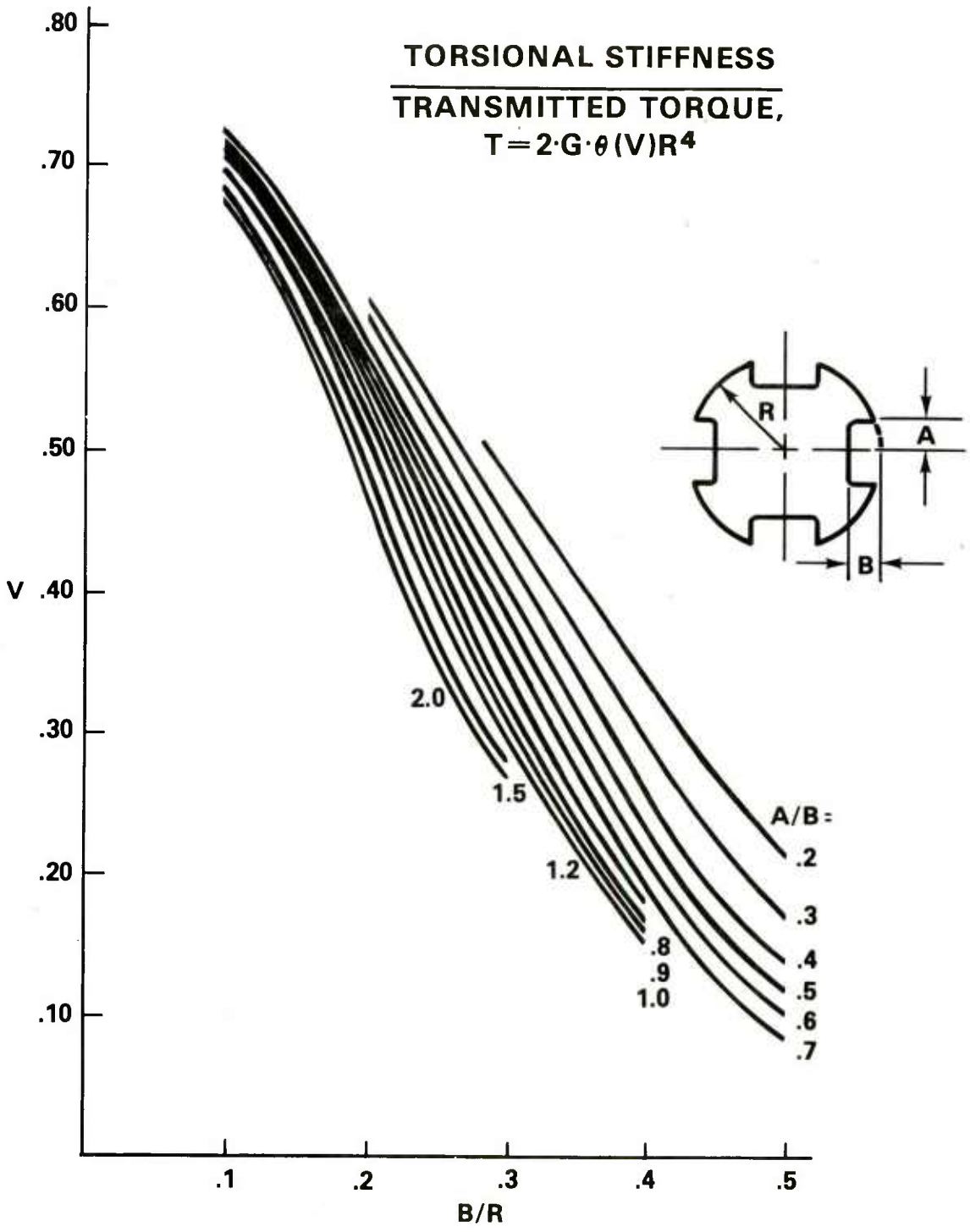

Figure 8. Four keyway shaft, torque.

Table 8. Four keyway shaft, volume factor (V)

A/B	B/R				
	0.1	0.2	0.3	0.4	0.5
0.2			.4806	.3361	.2114
0.3		.6088	.4511	.2965	.1705
0.4		.5952	.4253	.2624	.1384
0.5	.7214	.5769	.3983	.2333	.1140
0.6	.7190	.5672	.3805	.2119	.0962
0.7	.7161	.5541	.3605	.1935	.0842
0.8	.7124	.5422	.3444	.1783	
0.9	.7080	.5330	.3304	.1662	
1.0	.7024	.5203	.3160	.1572	
1.2	.6982	.5051	.2974	.1482	
1.5	.6870	.4832	.2787		
2.0	.6748	.4622	.2692		

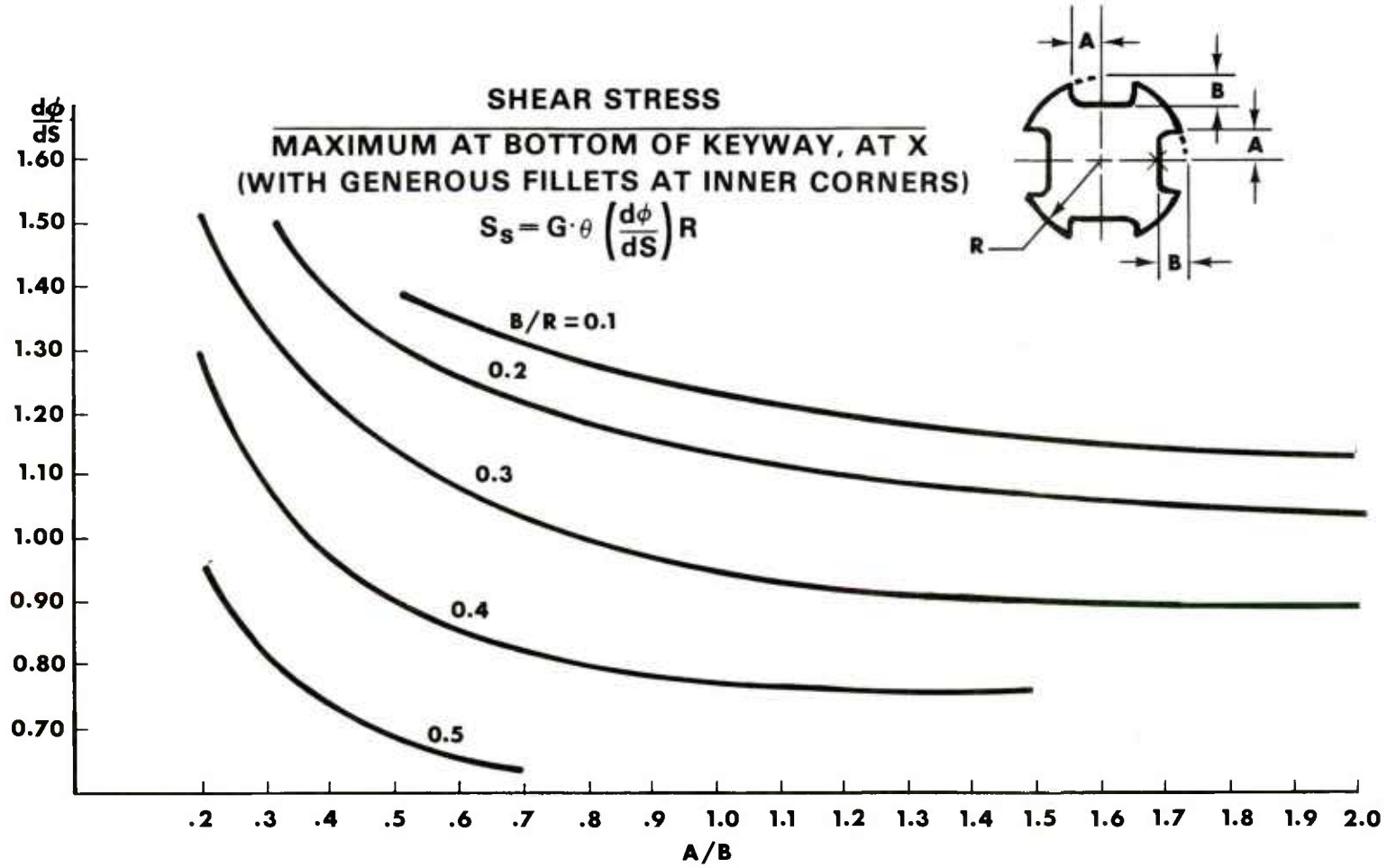

Figure 9. Four keyway shaft, stress.

Table 9. Four keyway shaft, slope factor ($d\Phi/ds$)

A/B	B/R				
	0.1	0.2	0.3	0.4	0.5
0.2			1.5127	1.2969	.9683
0.3		1.5096	1.3517	1.1047	.8172
0.4		1.4303	1.2333	.9849	.7300
0.5	1.3814	1.3158	1.1338	.9060	.6783
0.6	1.3648	1.2814	1.0903	.8624	.6486
0.7	1.3441	1.2326	1.0395	.8275	.6333
0.8	1.3181	1.1908	1.0072	.8016	
0.9	1.2848	1.1672	.9810	.7834	
1.0	1.2418	1.1325	.9557	.7715	
1.2	1.2239	1.1027	.9290	.7627	
1.5	1.1739	1.0638	.9054		
2.0	1.1376	1.0356	.8959		

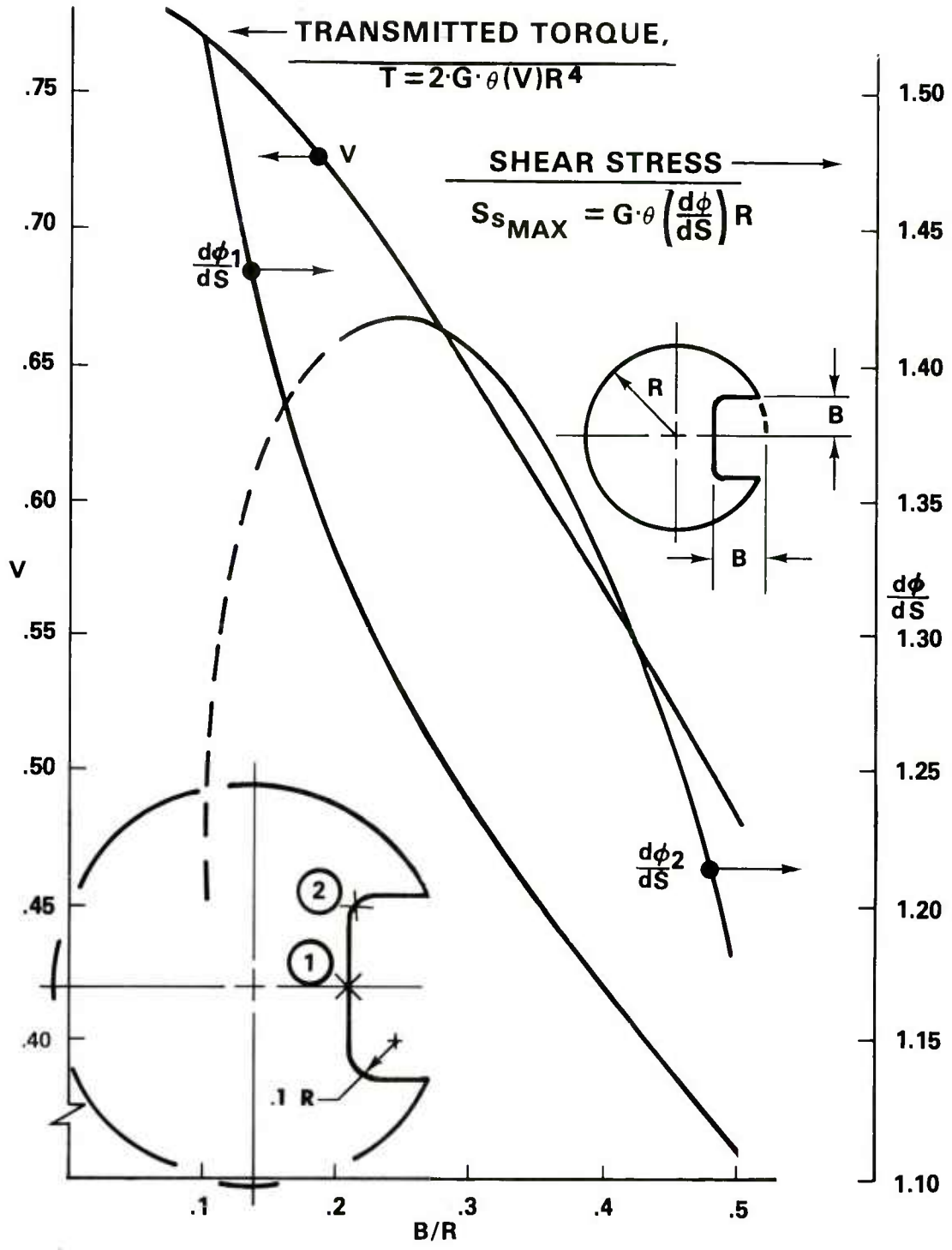

Figure 10. Single square keyway with inner fillets.

Table 10. Single square keyway with inner fillets

B/R	Volume factor (V)	Slope factor (dΦ/ds)	
		At keyway center (1)	At inner fillet (2)
0.1	.7703	1.5180	1.2024
0.2	.7206	1.3308	1.4091
0.3	.6504	1.2397	1.4072
0.4	.5690	1.1716	1.3249
0.5	.4840	1.1103	1.1854

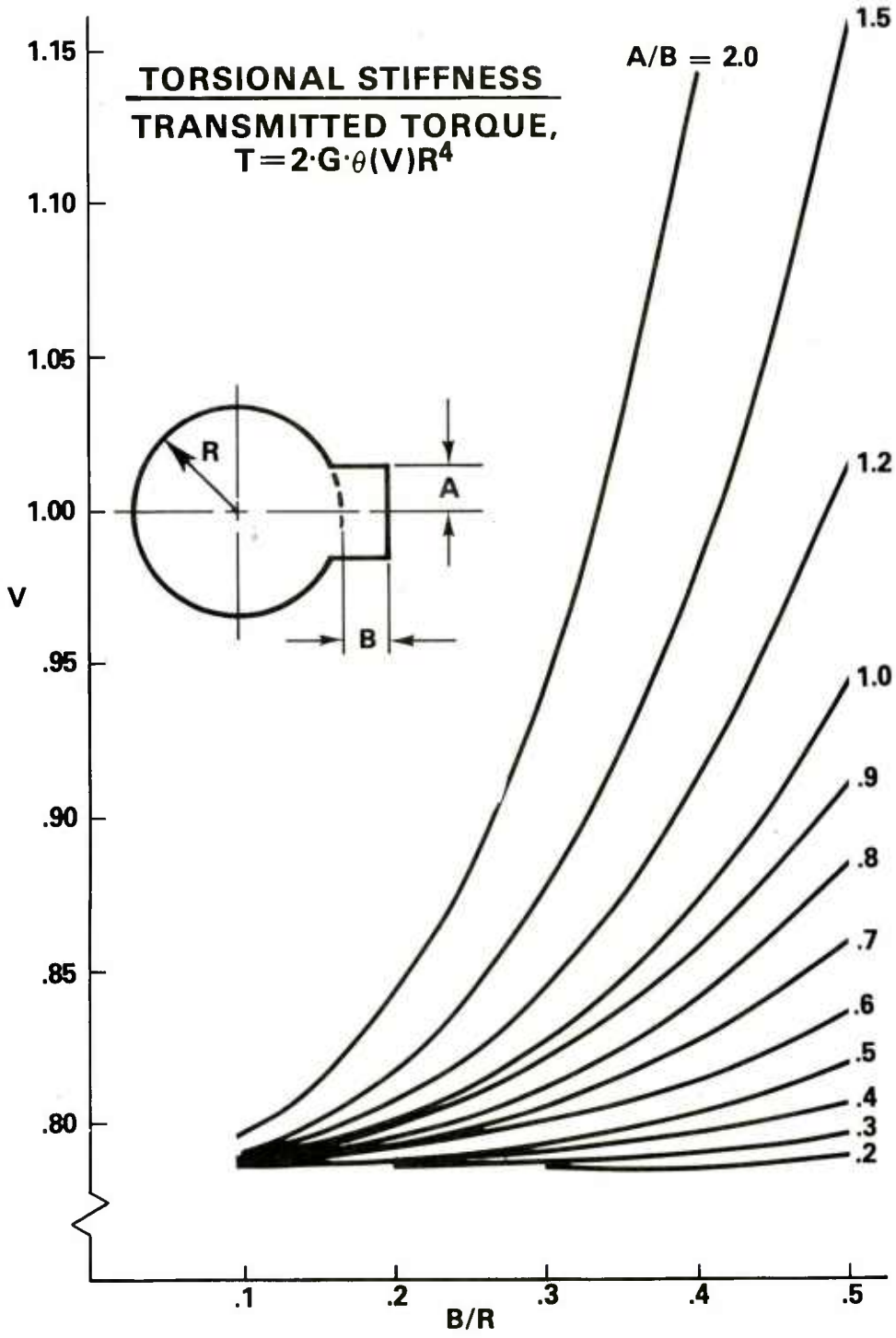

Figure 11. Single spline shaft, torque.

Table 11. Single spline shaft, volume factor (V)

A/B	B/R				
	0.1	0.2	0.3	0.4	0.5
0.2			.7853	.7865	.7878
0.3		.7853	.7870	.7906	.7944
0.4		.7864	.7903	.7968	.8048
0.5	.7845	.7874	.7933	.8035	.8189
0.6	.7852	.7899	.7993	.8143	.8362
0.7	.7857	.7918	.8059	.8270	.8580
0.8	.7862	.7950	.8113	.8390	.8832
0.9	.7866	.7976	.8202	.8560	.9110
1.0	.7869	.7996	.8253	.8712	.9433
1.2	.7890	.8071	.8456	.9117	1.0158
1.5	.7907	.8174	.8754	.9800	1.1561
2.0	.7953	.8407	.9420	1.1404	

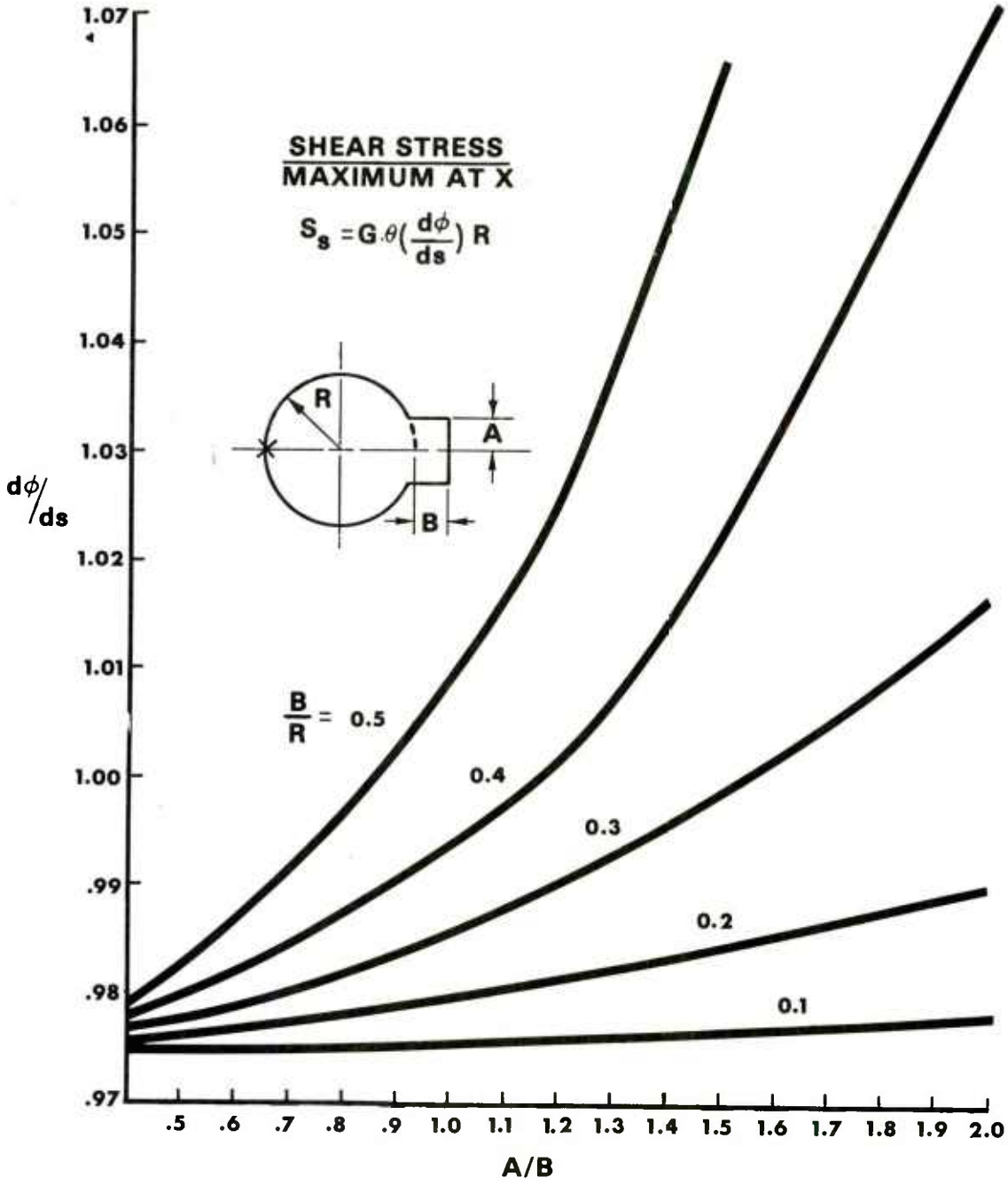

Figure 12. Single spline shaft, stress.

Table 12. Single spline shaft, slope factor ($d\Phi/ds$)

A/B	B/R				
	0.1	0.2	0.3	0.4	0.5
0.2			.9753	.9757	.9759
0.3		.9753	.9758	.9767	.9774
0.4		.9757	.9767	.9782	.9797
0.5	.9751	.9759	.9773	.9796	.9827
0.6	.9753	.9767	.9789	.9823	.9864
0.7	.9754	.9771	.9807	.9853	.9912
0.8	.9756	.9780	.9820	.9879	.9966
0.9	.9757	.9787	.9843	.9921	1.0028
1.0	.9758	.9792	.9854	.9954	1.0100
1.2	.9765	.9813	.9908	1.0055	1.0272
1.5	.9769	.9841	.9984	1.0228	1.0646
2.0	.9782	.9906	1.0169	1.0714	

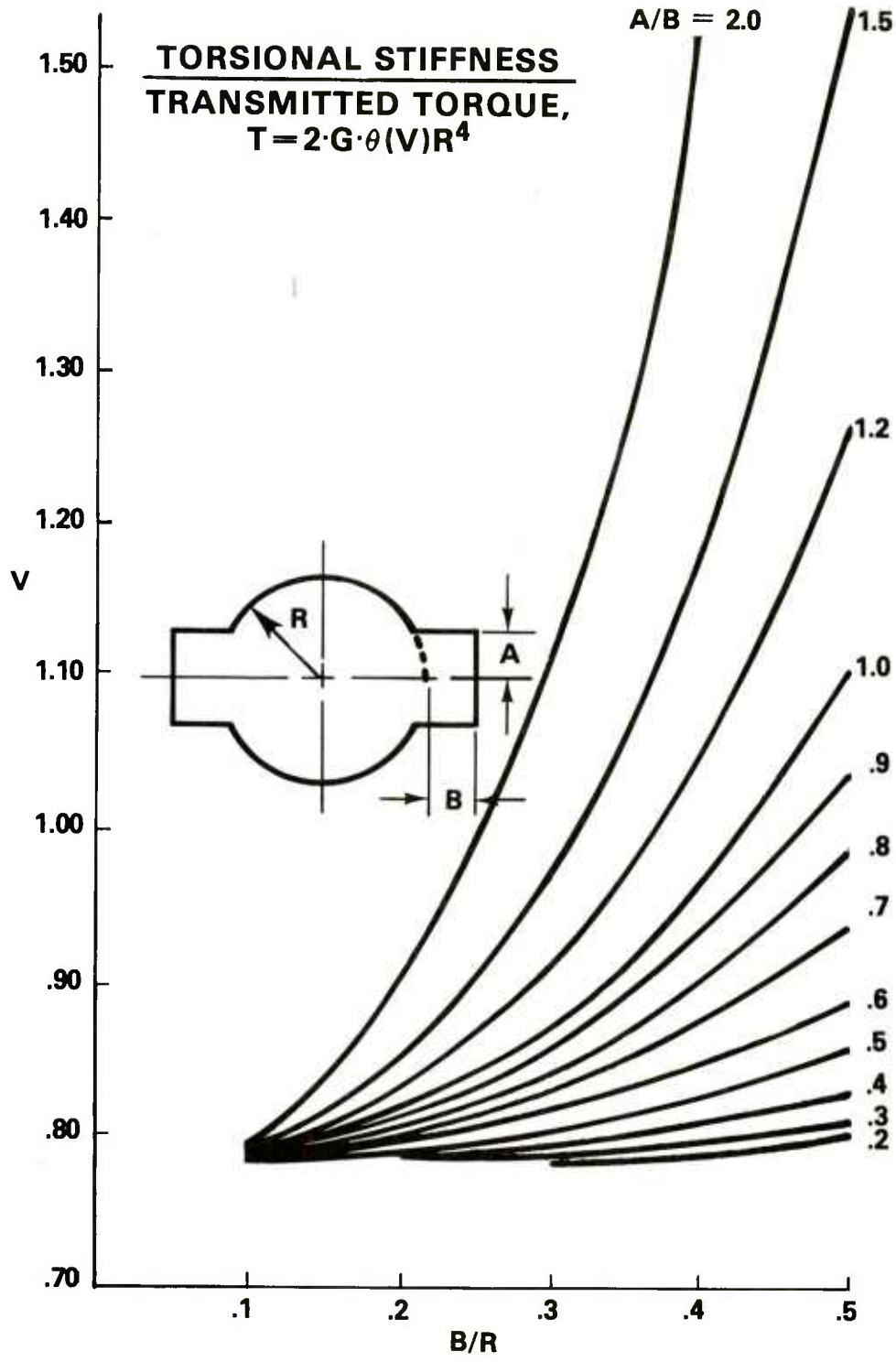

Figure 13. Two spline shaft, torque.

Table 13. Two spline shaft, volume factor (V)

A/B	B/R				
	0.1	0.2	0.3	0.4	0.5
0.2			.7865	.7889	.7914
0.3		.7864	.7899	.7970	.8047
0.4		.7886	.7965	.8095	.8255
0.5	.7850	.7906	.8026	.8229	.8538
0.6	.7863	.7958	.8145	.8446	.8886
0.7	.7874	.7994	.8278	.8701	.9326
0.8	.7883	.8059	.8386	.8945	.9837
0.9	.7891	.8111	.8565	.9288	1.0400
1.0	.7897	.8152	.8668	.9595	1.1058
1.2	.7940	.8302	.9078	1.0418	1.2547
1.5	.7973	.8509	.9682	1.1818	1.5471
2.0	.8066	.8980	1.1045	1.5172	

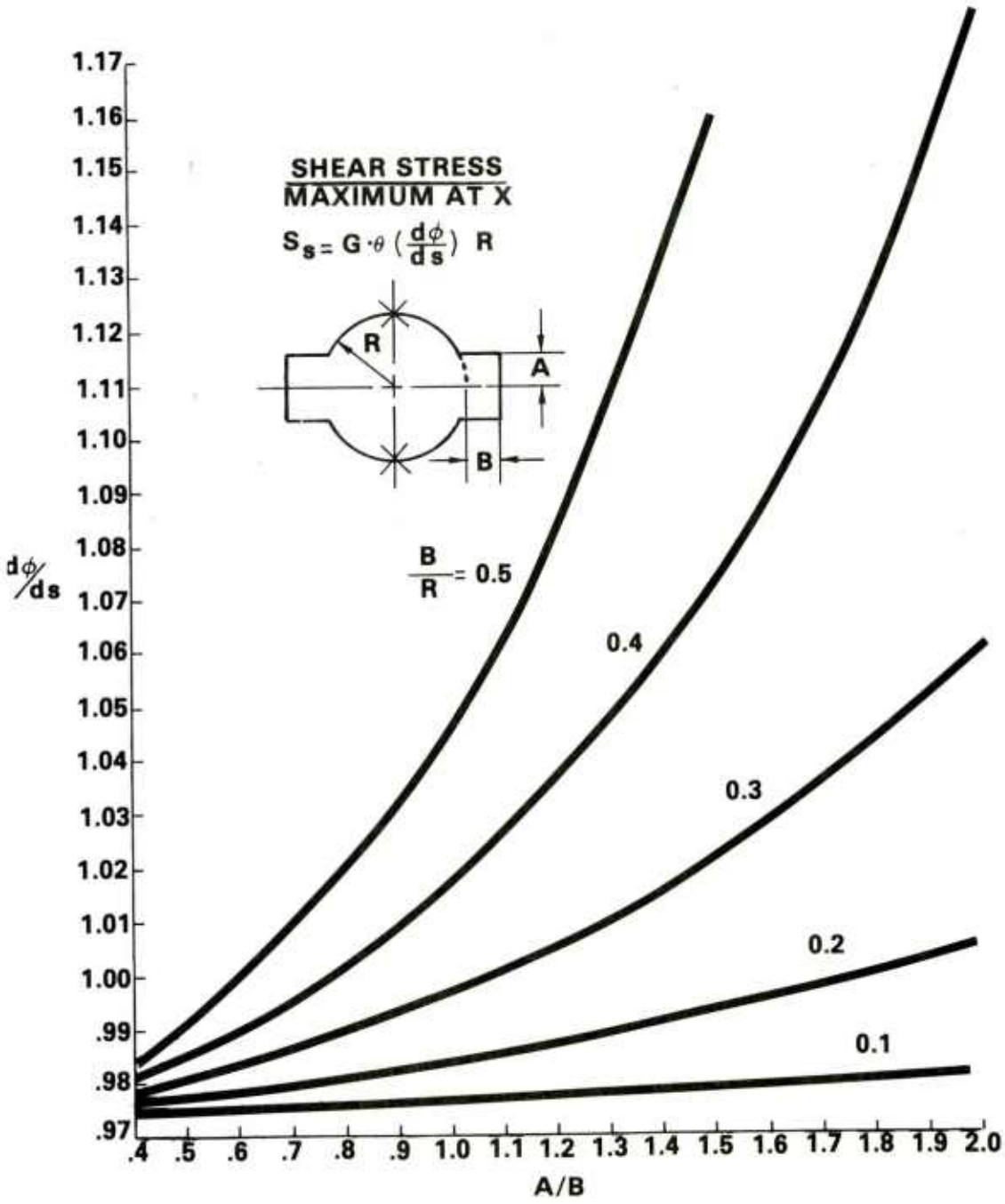

Figure 14. Two spline shaft, stress.

Table 14. Two spline shaft, slope factor ($d\Phi/ds$)

A/B	B/R				
	0.1	0.2	0.3	0.4	0.5
0.2			.9757	.9763	.9769
0.3		.9757	.9766	.9784	.9799
0.4		.9763	.9784	.9815	.9845
0.5	.9753	.9768	.9799	.9844	.9906
0.6	.9757	.9783	.9830	.9896	.9980
0.7	.9760	.9793	.9864	.9956	1.0076
0.8	.9763	.9811	.9890	1.0011	1.0187
0.9	.9765	.9825	.9937	1.0094	1.0312
1.0	.9767	.9836	.9959	1.0164	1.0462
1.2	.9780	.9877	1.0068	1.0367	1.0812
1.5	.9789	.9933	1.0222	1.0722	1.1595
2.0	.9817	1.0066	1.0601	1.1739	

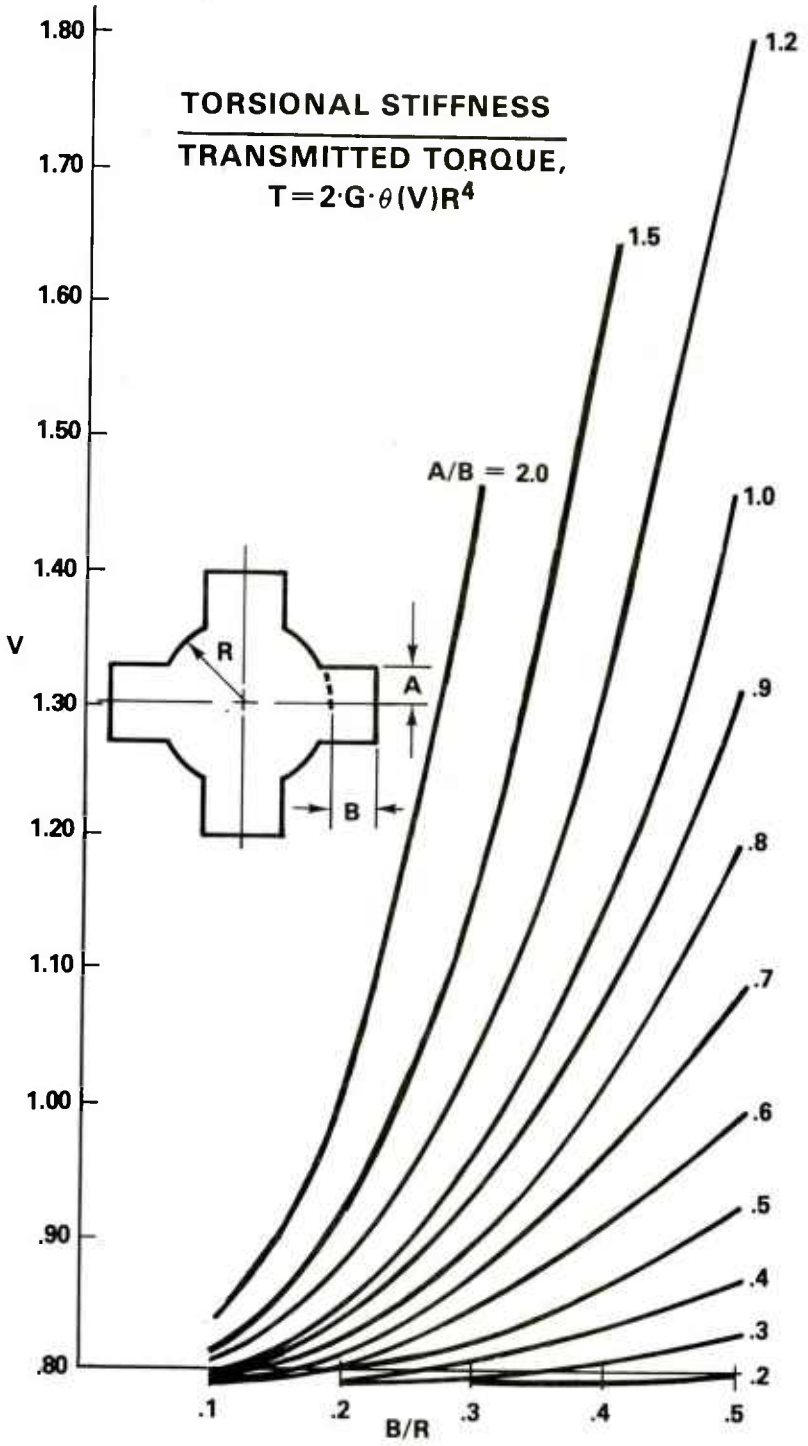

Figure 15. Four spline shaft, torque.

Table 15. Four spline shaft, volume factor (V)

A/B	B/R				
	0.1	0.2	0.3	0.4	0.5
0.2			.7888	.7937	.7989
0.3		.7887	.7957	.8101	.8254
0.4		.7932	.8090	.8352	.8674
0.5	.7859	.7971	.8213	.8623	.9250
0.6	.7885	.8076	.8452	.9063	.9962
0.7	.7906	.8149	.8723	.9588	1.0877
0.8	.7924	.8280	.8944	1.0090	1.1950
0.9	.7940	.8386	.9310	1.0808	1.3158
1.0	.7954	.8467	.9519	1.1455	1.4601
1.2	.8040	.8773	1.0378	1.3239	1.8021
1.5	.8106	.9196	1.1663	1.6438	
2.0	.8292	1.0180	1.4739		

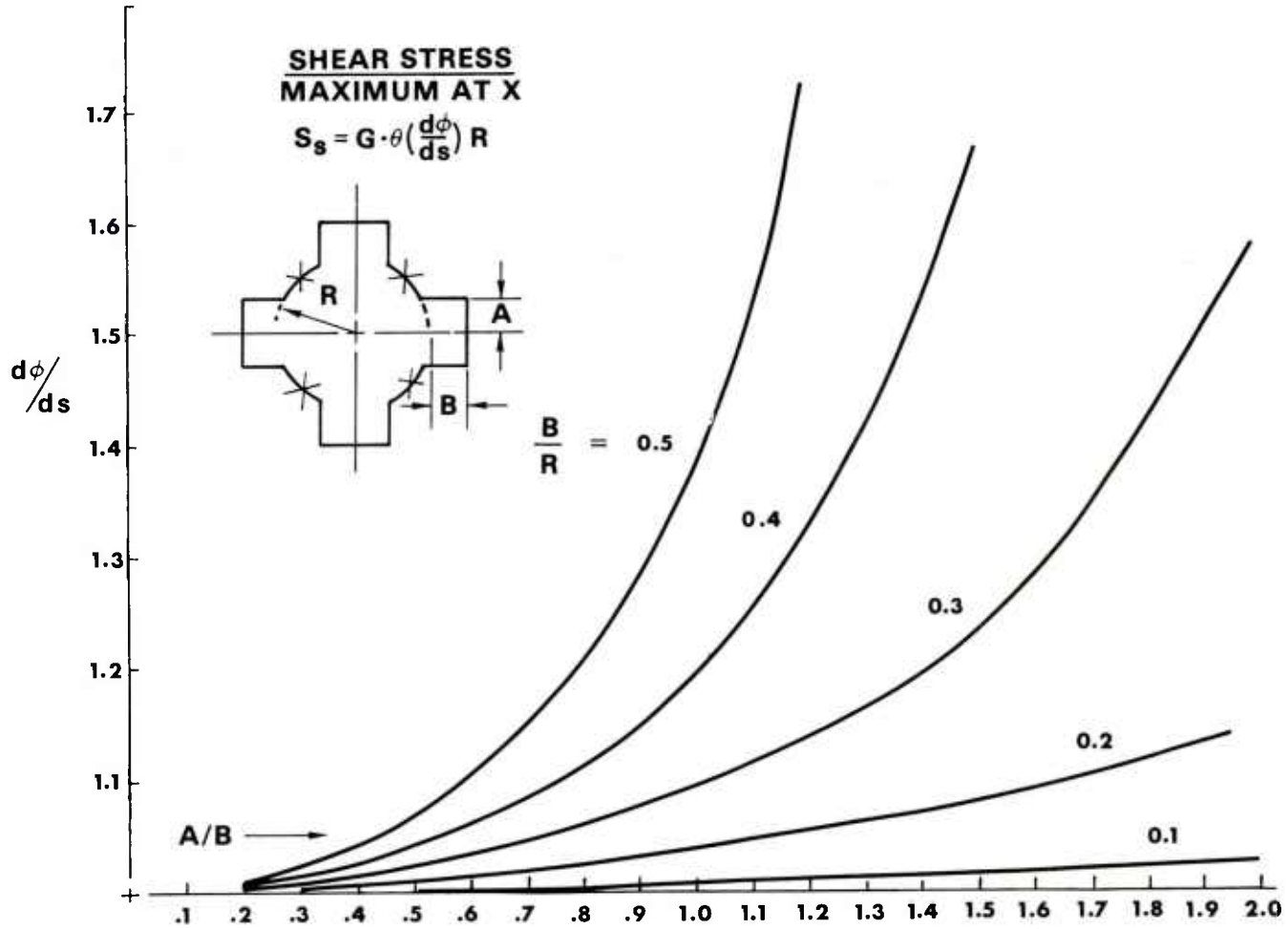

Figure 16. Four spline shaft, stress.

Table 16. Four spline shaft, slope factor ($d\Phi/ds$)

A/B	B/R				
	0.1	0.2	0.3	0.4	0.5
0.2			1.0027	1.0052	1.0073
0.3		1.0027	1.0063	1.0135	1.0196
0.4		1.0052	1.0134	1.0260	1.0385
0.5	1.0010	1.0072	1.0193	1.0381	1.0646
0.6	1.0026	1.0132	1.0321	1.0601	1.0978
0.7	1.0039	1.0170	1.0469	1.0873	1.1436
0.8	1.0050	1.0246	1.0578	1.1131	1.2019
0.9	1.0059	1.0304	1.0788	1.1552	1.2743
1.0	1.0066	1.0346	1.0890	1.1911	1.3766
1.2	1.0118	1.0525	1.1432	1.3210	1.7211
1.5	1.0156	1.0778	1.2313	1.6632	
2.0	1.0270	1.1463	1.5858		

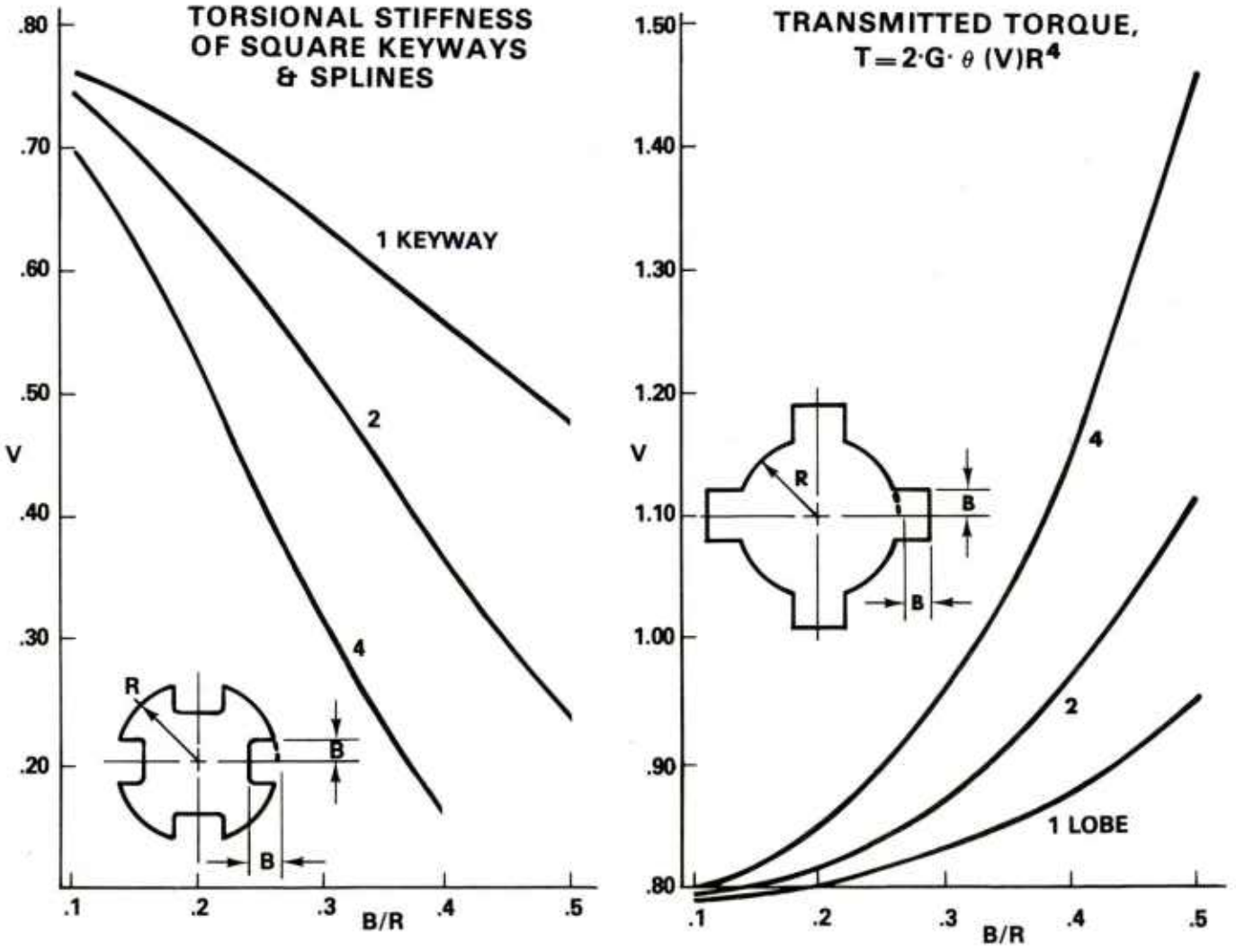

Figure 17. Square keyways and external splines, torque.

Table 17. Square keyways and external splines, volume factor (V)

B/R	One keyway	Two keyways	Four keyways
0.1	.7633	.7426	.7024
0.2	.7125	.6433	.5203
0.3	.6424	.5117	.3160
0.4	.5619	.3713	.1572
0.5	.4783	.2416	

B/R	One spline	Two splines	Four splines
0.1	.7869	.7897	.7954
0.2	.7996	.8152	.8467
0.3	.8253	.8668	.9519
0.4	.8712	.9595	1.1455
0.5	.9433	1.1058	1.4601

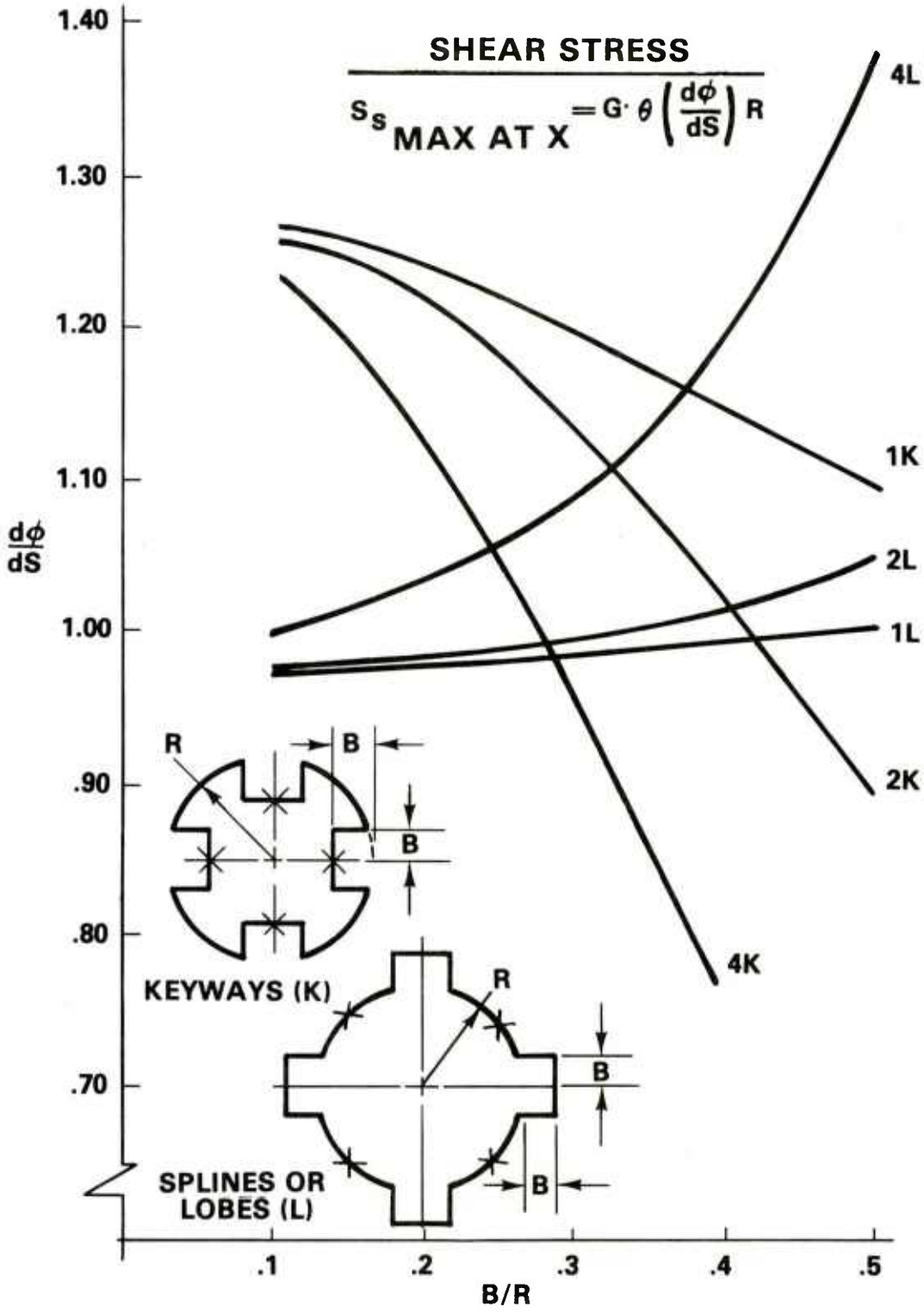

Figure 18. Square keyways and external splines, stress.

Table 18. Square keyways and external splines, slope factor ($d\Phi/ds$)

B/R	One keyway	Two keyways	Four keyways
0.1	1.2698	1.2641	1.2418
0.2	1.2469	1.2216	1.1325
0.3	1.2022	1.1392	.9557
0.4	1.1524	1.0297	.7715
0.5	1.1002	.8930	

B/R	One Spline	Two splines	Four splines
0.1	.9758	.9767	1.0066
0.2	.9792	.9836	1.0346
0.3	.9854	.9959	1.0890
0.4	.9954	1.0164	1.1911
0.5	1.0100	1.0462	1.3766

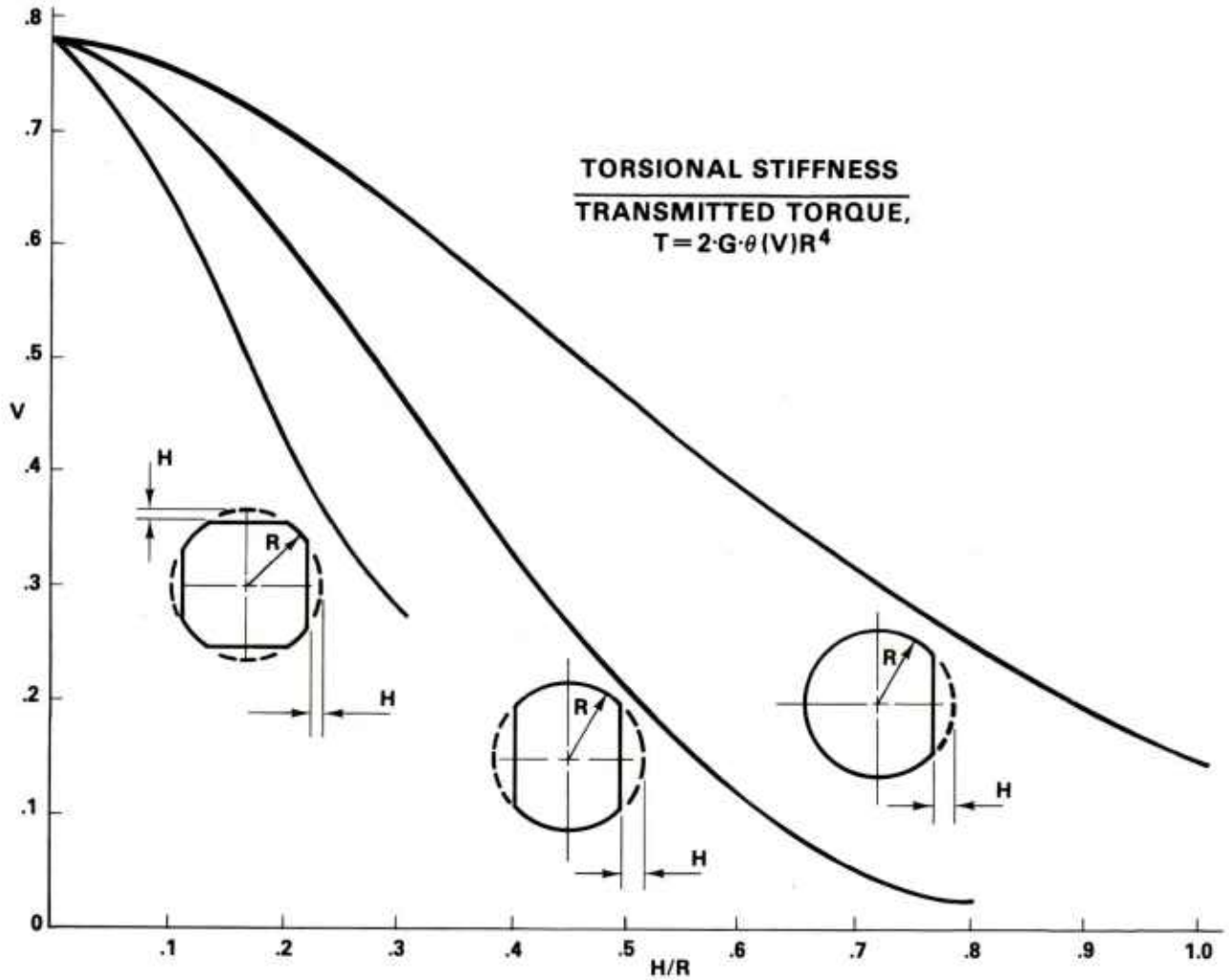

Figure 19. Milled shaft, torque.

Table 19. Milled shaft, volume factor (V)

H/R	One flat	Two flats	Four flats
0	.7813	.7811	.7811
0.1	.7617	.7149	.6520
0.2	.7018	.5998	.4501
0.29289			.2777
0.3	.6291	.4667	
0.4	.5510	.3349	
0.5	.4717	.2168	
0.6	.3951	.1225	
0.7	.3228	.0559	
0.8	.2568	.0173	
0.9	.1980		
1.0	.1460		

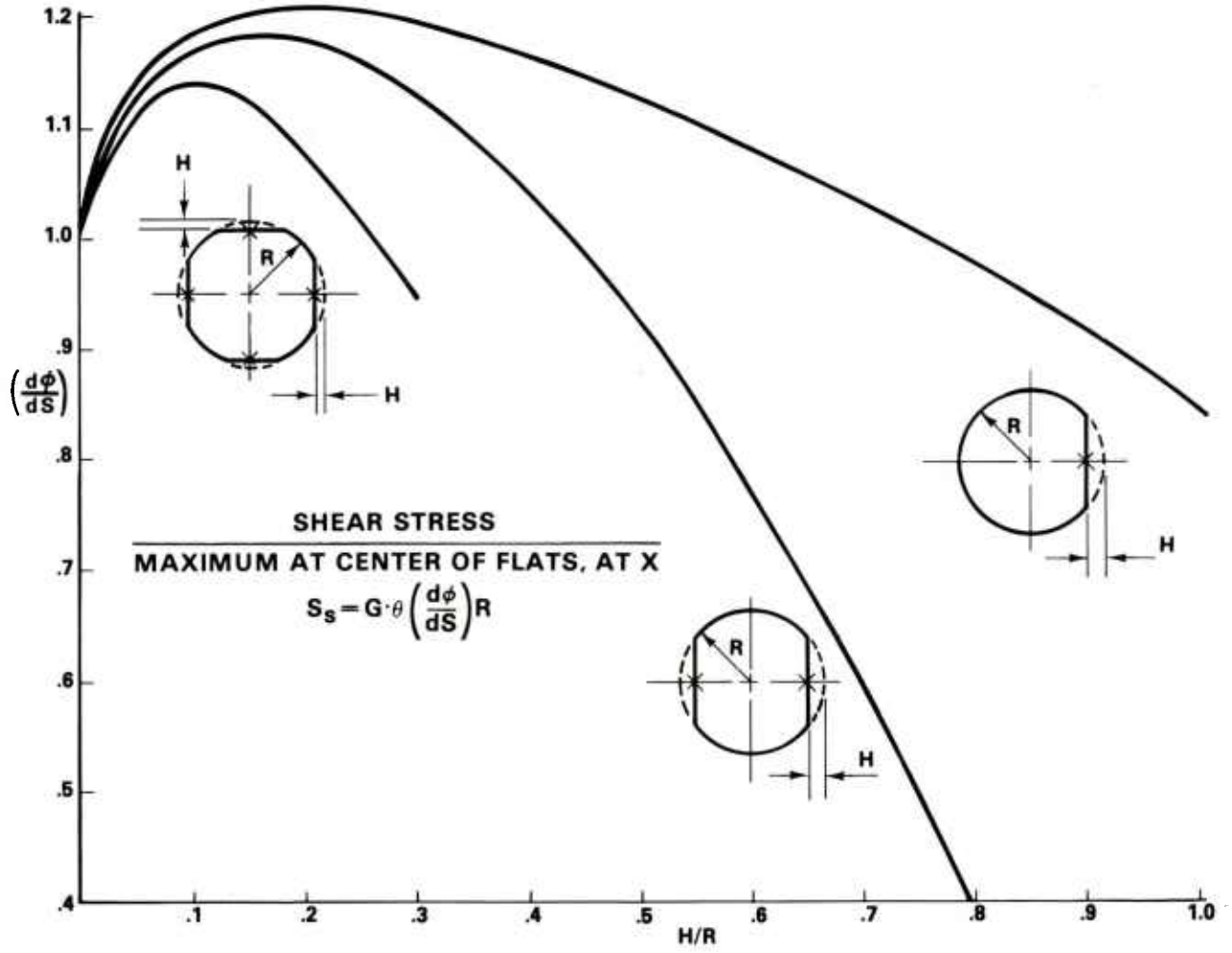

Figure 20. Milled shaft, stress.

Table 20. Milled shaft, slope factor ($d\Phi/ds$)

H/R	One flat	Two flats	Four flats
0	1.0	1.0	1.0
0.1	1.1870	1.1788	1.1465
0.2	1.2078	1.1773	1.0718
0.29289			.9507
0.3	1.1975	1.1279	
0.4	1.1710	1.0423	
0.5	1.1333	.9227	
0.6	1.0876	.7717	
0.7	1.0352	.5940	
0.8	.9773	.3996	
0.9	.9148		
1.0	.8457		

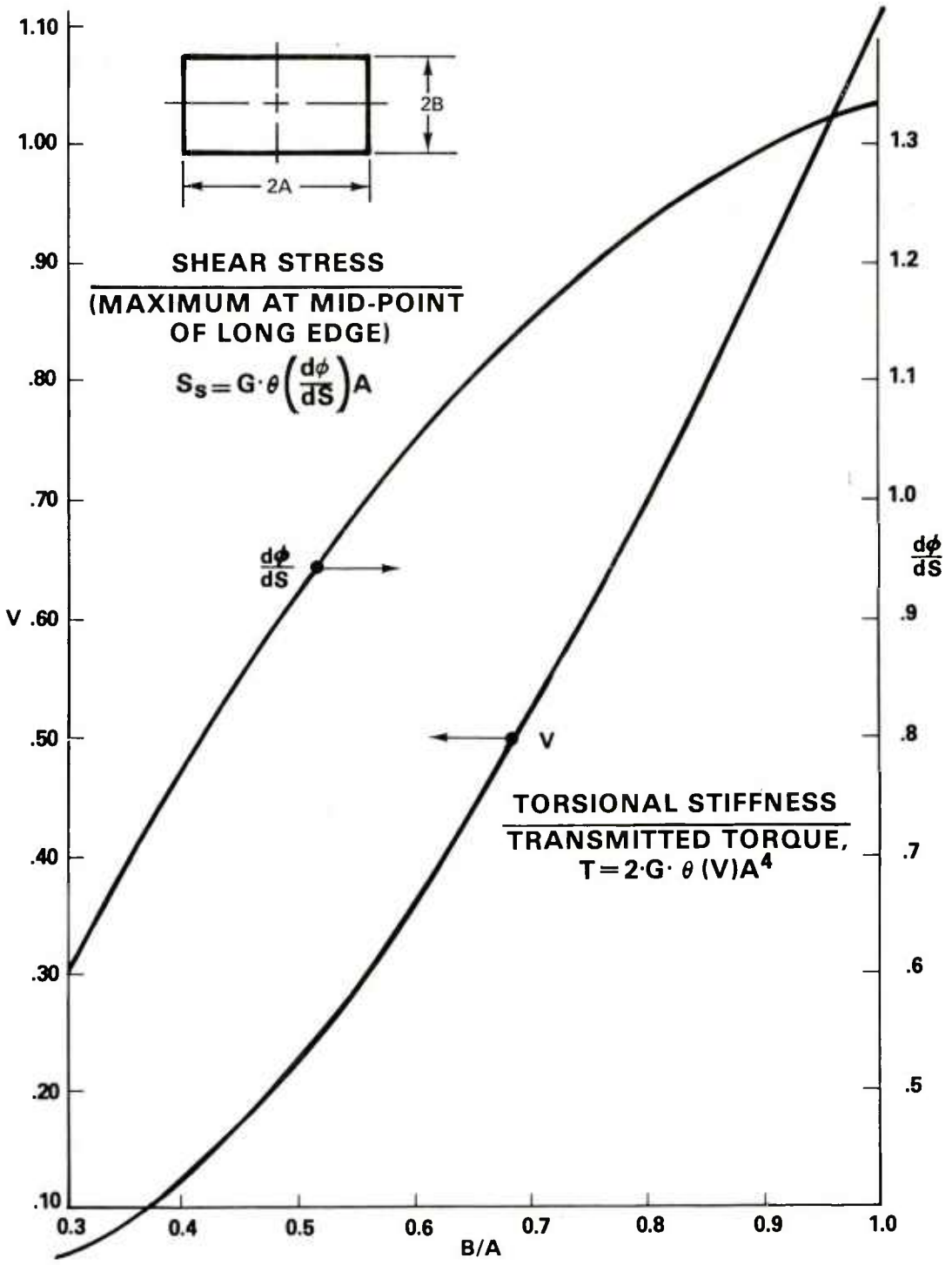

Figure 21. Rectangular shaft.

Table 21. Rectangular shaft

B/A	Volume factor (V)	Slope factor ($d\Phi/ds$)
0.3	.05635	.5942
0.4	.1248	.7731
0.5	.2250	.9280
0.6	.3559	1.0563
0.7	.5146	1.1589
0.8	.6971	1.2391
0.9	.8991	1.3008
1.0	1.1167	1.3475

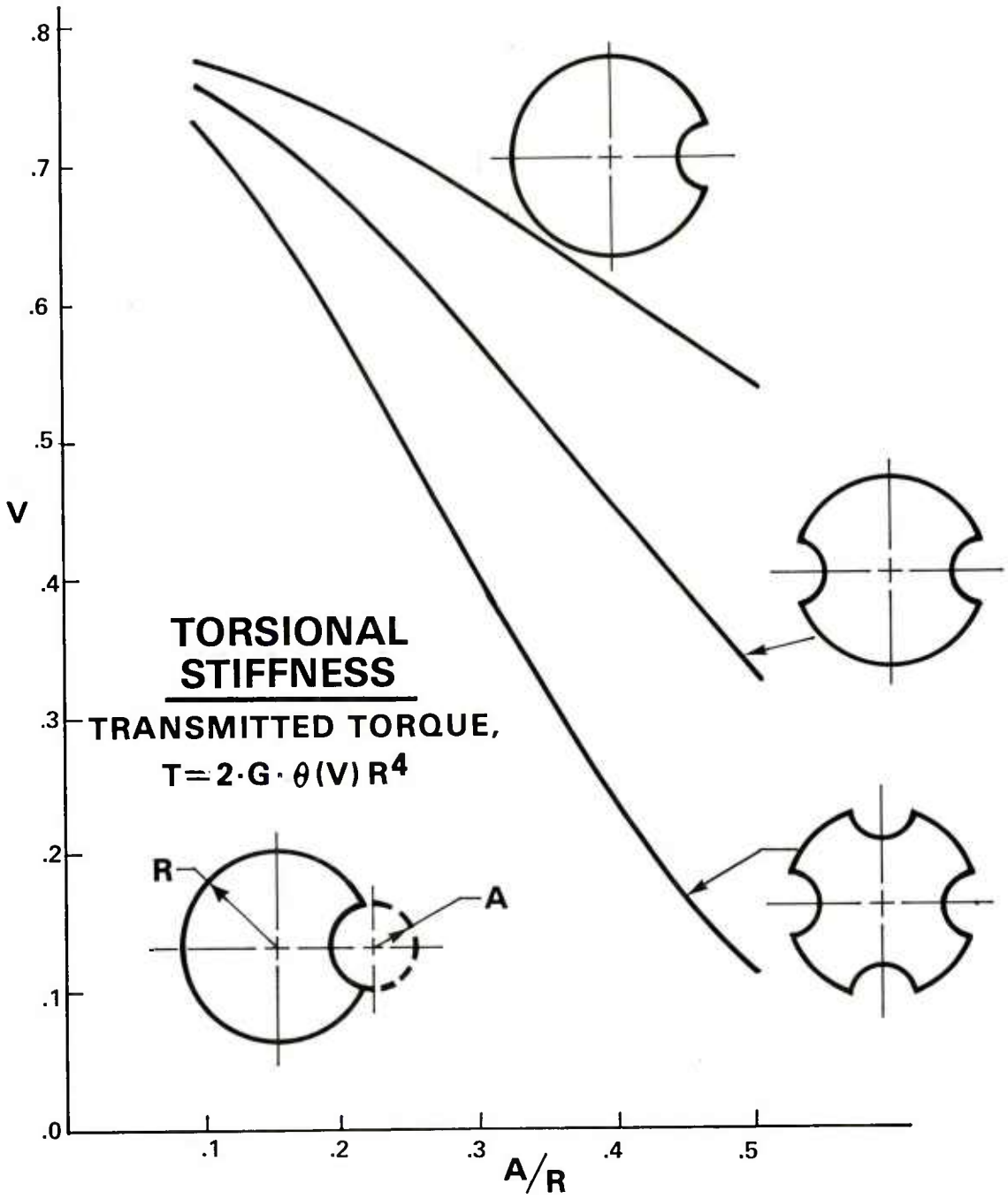

Figure 22. Pinned shaft, torque.

Table 22. Pinned shaft, volume factor (V)

A/R	One groove	Two grooves	Four grooves
0.1	.7700	.7558	.7280
0.2	.7316	.6803	.5855
0.3	.6760	.5738	.4062
0.4	.6087	.4521	.2374
0.5	.5349	.3300	.1118

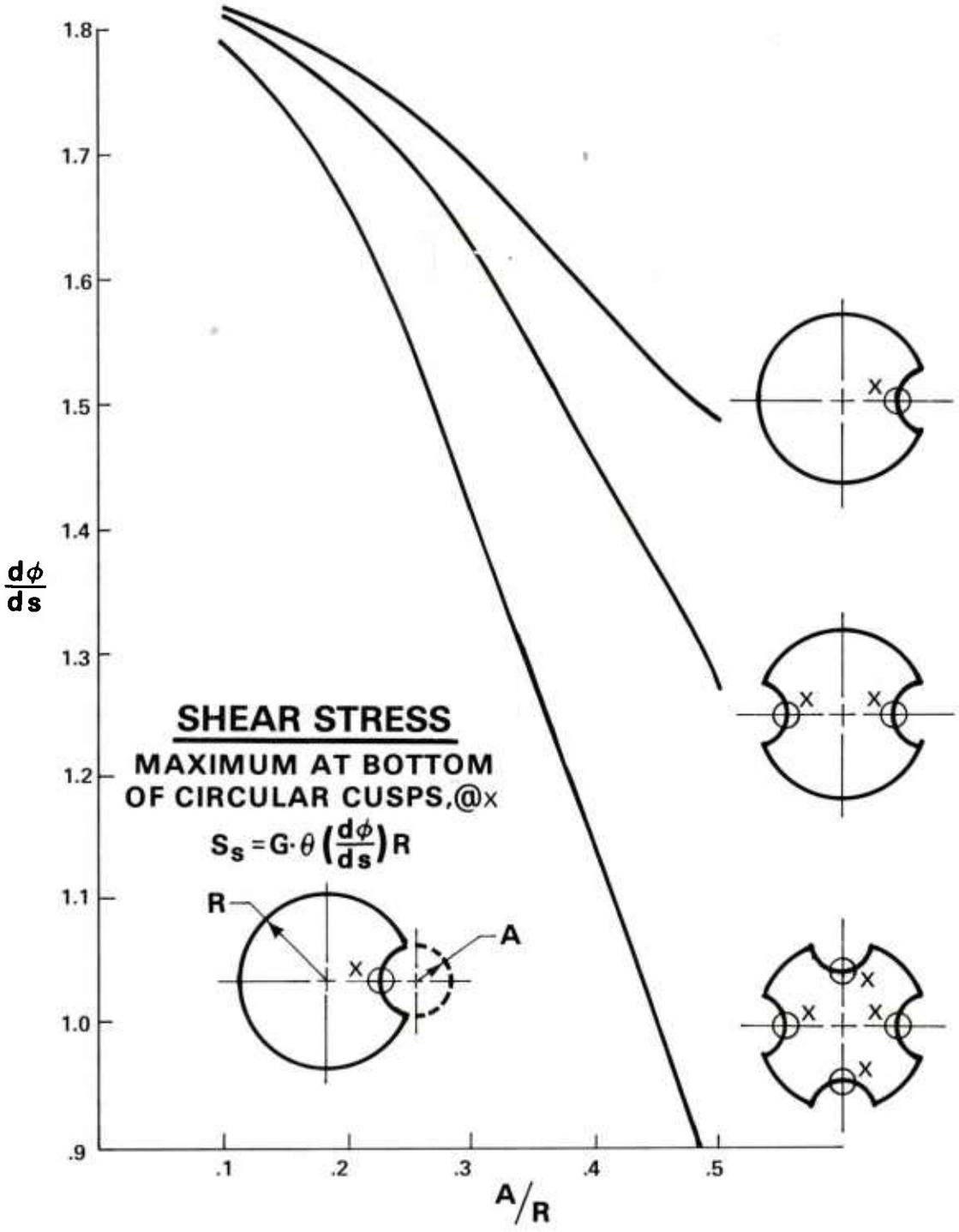

Figure 23. Pinned shaft, stress.

Table 23. Pinned shaft, slope factor ($d\Phi/ds$)

A/R	One groove	Two grooves	Four grooves
0.1	1.8164	1.3111	1.7907
0.2	1.7698	1.7452	1.6558
0.3	1.6852	1.6229	1.4249
0.4	1.5831	1.4603	1.1441
0.5	1.4878	1.2753	0.8728

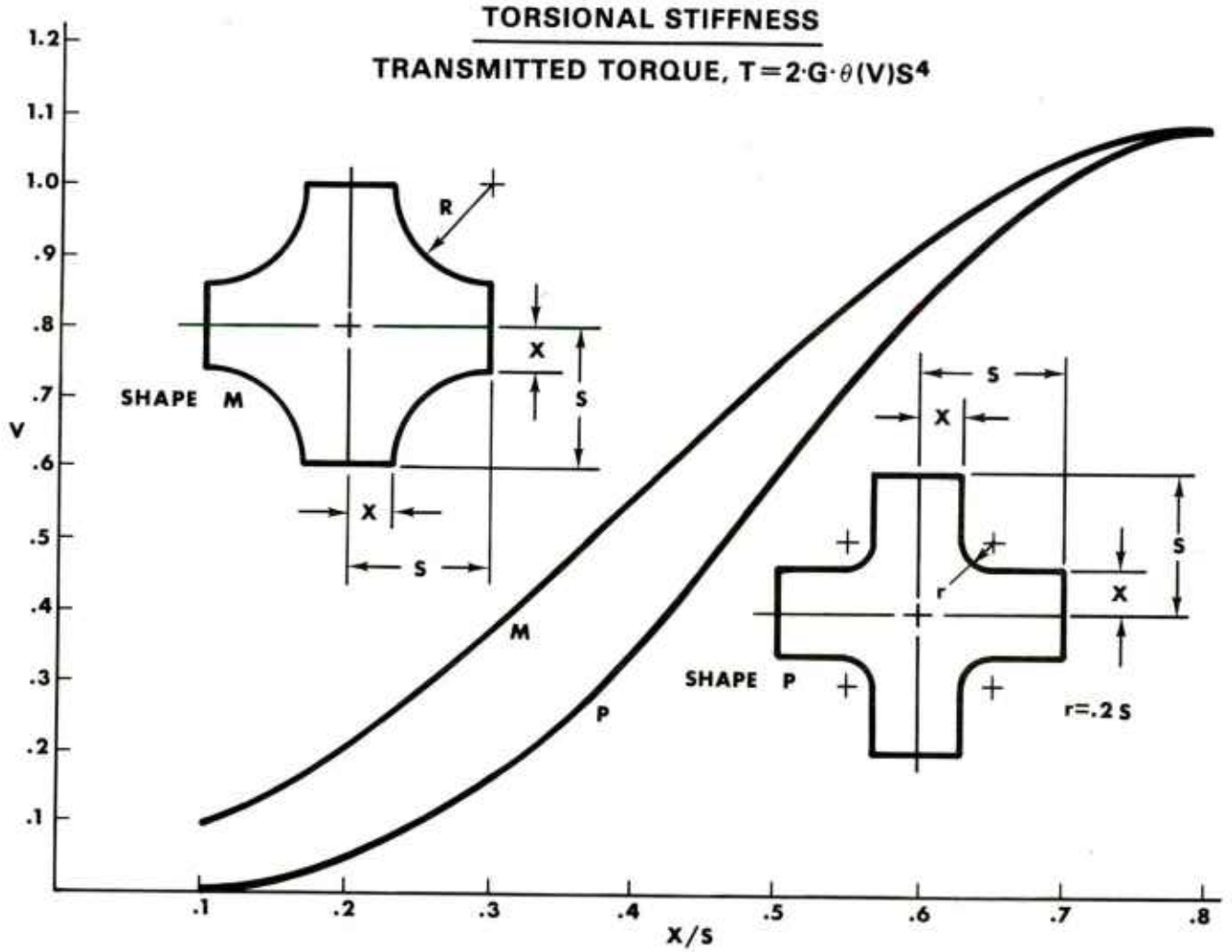

Figure 24. Cross shaft, torque.

Table 24. Cross shaft, volume factor (V)

X/S	Shape P	Shape M
0.1	.00741	.09907
0.2	.05219	.2120
0.3	.1642	.3767
0.4	.3538	.5714
0.5	.5947	.7639
0.6	.8302	.9247
0.7	1.0058	1.0368
0.8	1.0981	1.0981

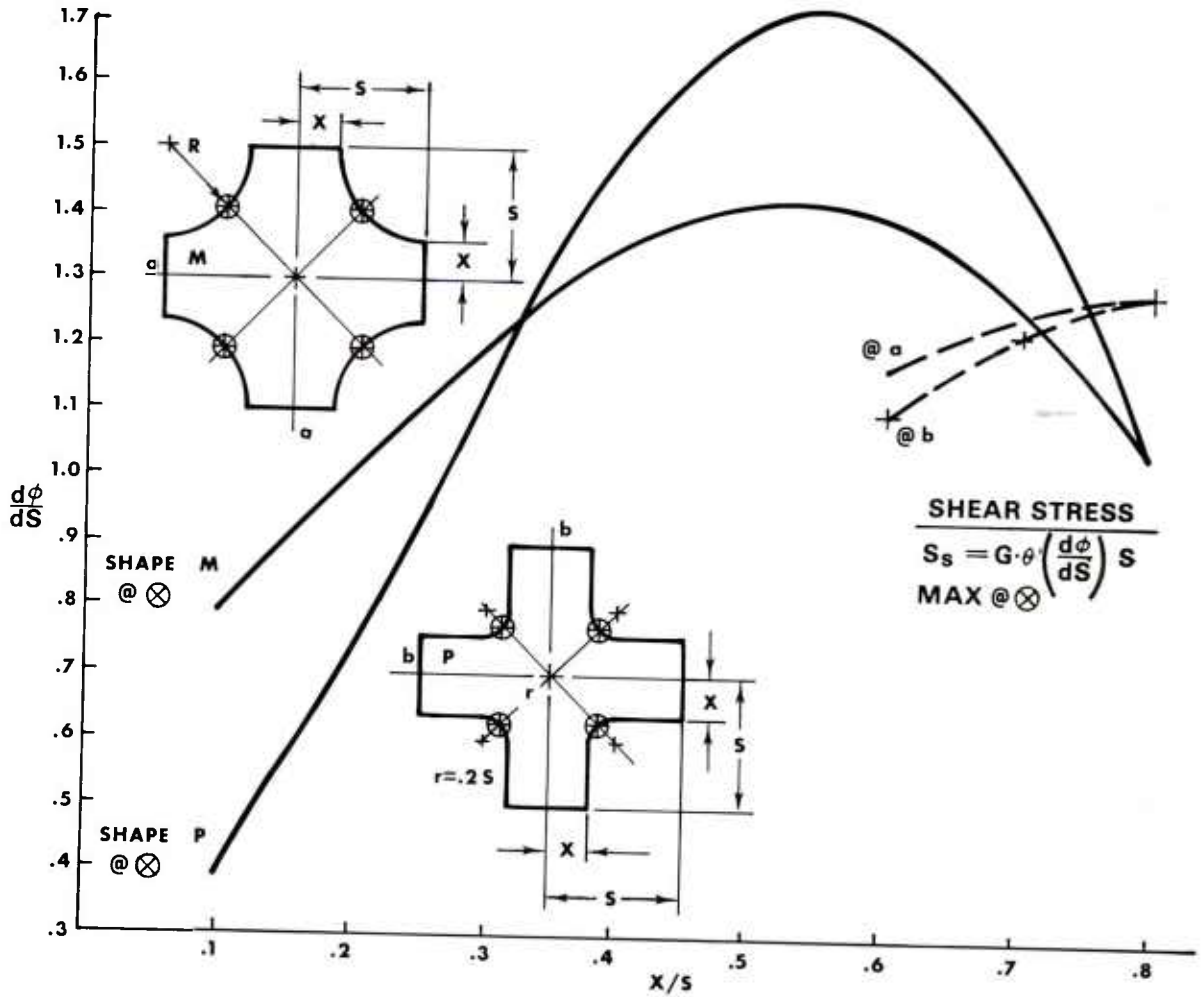

Figure 25. Cross shaft, stress.

Table 25. Cross shaft, slope factor ($d\Phi/ds$)

X/S	Shape P		Shape M	
	At x	At b	At x	At a
0.1	.3986	.1036	.8060	.1280
0.2	.7615	.2514	1.0051	.3589
0,3	1.1577	.4247	1.1917	.6139
0.4	1.4997	.6450	1.3535	.8503
0.5	1.6925	.8901	1.4071	1.0416
0.6	1.6795	1.1007	1.4011	1.1755
0.7	1.4573	1.2335	1.2563	1.2539
0.8	1.0460	1.2896	1.0460	1.2896

ACCURACY OF THE COMPUTERIZED SOLUTION

To compare the CLYDE (computer) analysis of the torsion of a solid circular shaft with the exact, classical textbook solution, one quadrant of a unit-radius shaft was run with two finite-difference grid spacings and the results of the equations were compared, as follows:

Equation Comparison	CLYDE		Exact
Torque	$2G\theta(V)R^4$	$\longleftrightarrow$	$G\theta J$
	$2(V)R^4$	$\longleftrightarrow$	J
	$2(V)R^4$	$\longleftrightarrow$	$(\pi/2)R^4$
	$2V$	$\longleftrightarrow$	$(\pi/2)$
Shear stress (max)	$G\theta(\frac{d\Phi}{ds})R$	$\longleftrightarrow$	$G\theta R$
	$(\frac{d\Phi}{ds})$	$\longleftrightarrow$	1.

		CLYDE	Exact	Deviation (%)
Torque	(h=0.125)	1.5546	1.5708	1.03
	(h=0.0625)	1.5669	1.5708	0.25
Shear stress	(h=0.125)	0.9379	1.0	6.21
	(h=0.0625)	0.9688	1.0	3.125
Area*	(h=0.125)	3.13316	3.14159	0.268
	(h=0.0625)	3.13984	3.14159	0.056

*Used for internal program checking.

The mathematical model used in the CLYDE computer program is described in appendix A. A planned extension of the mathematical model is contained in appendix B.

PARALLEL SHAFT CONCEPT

The torsional rigidity of a uniform circular shaft, i.e., the torque required to produce unit (one radian) displacement, is:

$$C = T/\theta = G \cdot J$$

In the terminology of the membrane analogy, the torsional rigidity of non-circular shafts is defined as:

$$C = T/\theta = 2 \cdot G \cdot \theta (V) f(R)/\theta$$

The overall torsional rigidity of a system consisting of a number of shafts in parallel (fig. 26) is simply the sum of the torsional rigidities of the individual component shafts.

$$\sum_{i=1}^{N} C_i = C_1 + C_2 + C_3 + \cdots + C_N$$

$$\sum_{i=1}^{N} T_i\theta_i = \theta \sum_{i=1}^{N} T_i = \theta(T_1 + T_2 + T_3 + \cdots + T_N)$$

The torsional rigidity of hollow shafts can be determined by regarding the configuration as a parallel shaft arrangement. The overall torsional rigidity can be obtained by subtracting the torsional rigidity of a shaft having the dimensions of the bore (or inner contour) from that of a shaft having the dimensions of the outer contour. The advantages of being able to apply the principles of superposition (fig. 27-31) to combinations of concentric (inner and outer) shaft contours are obvious. If, for example, design charts have been prepared for 20 different shaft shapes, then 400 different solutions to all possible combinations of inner and outer shaft contours (20 inner x 20 outer) are available.

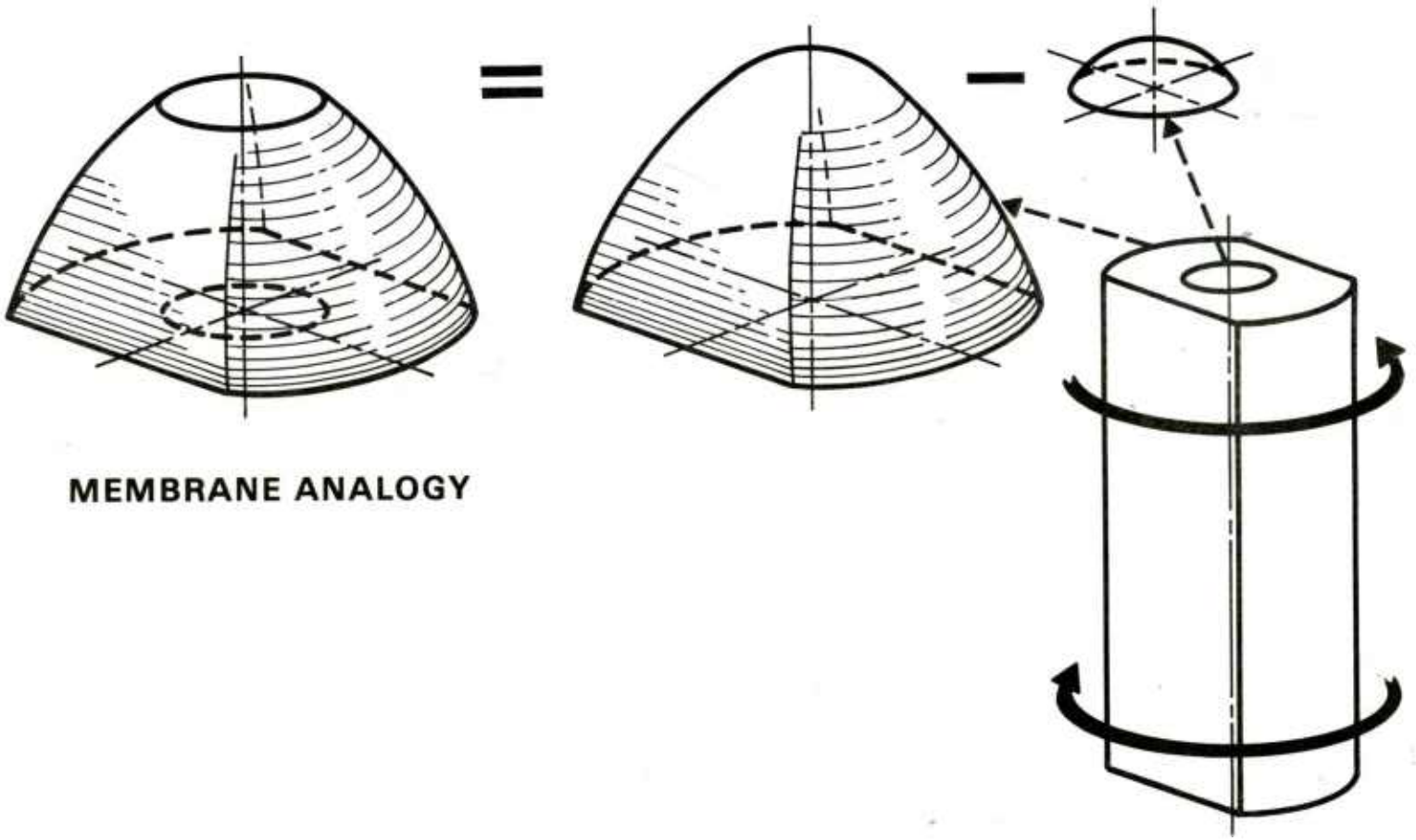

Figure 26. Parallel shaft concept.

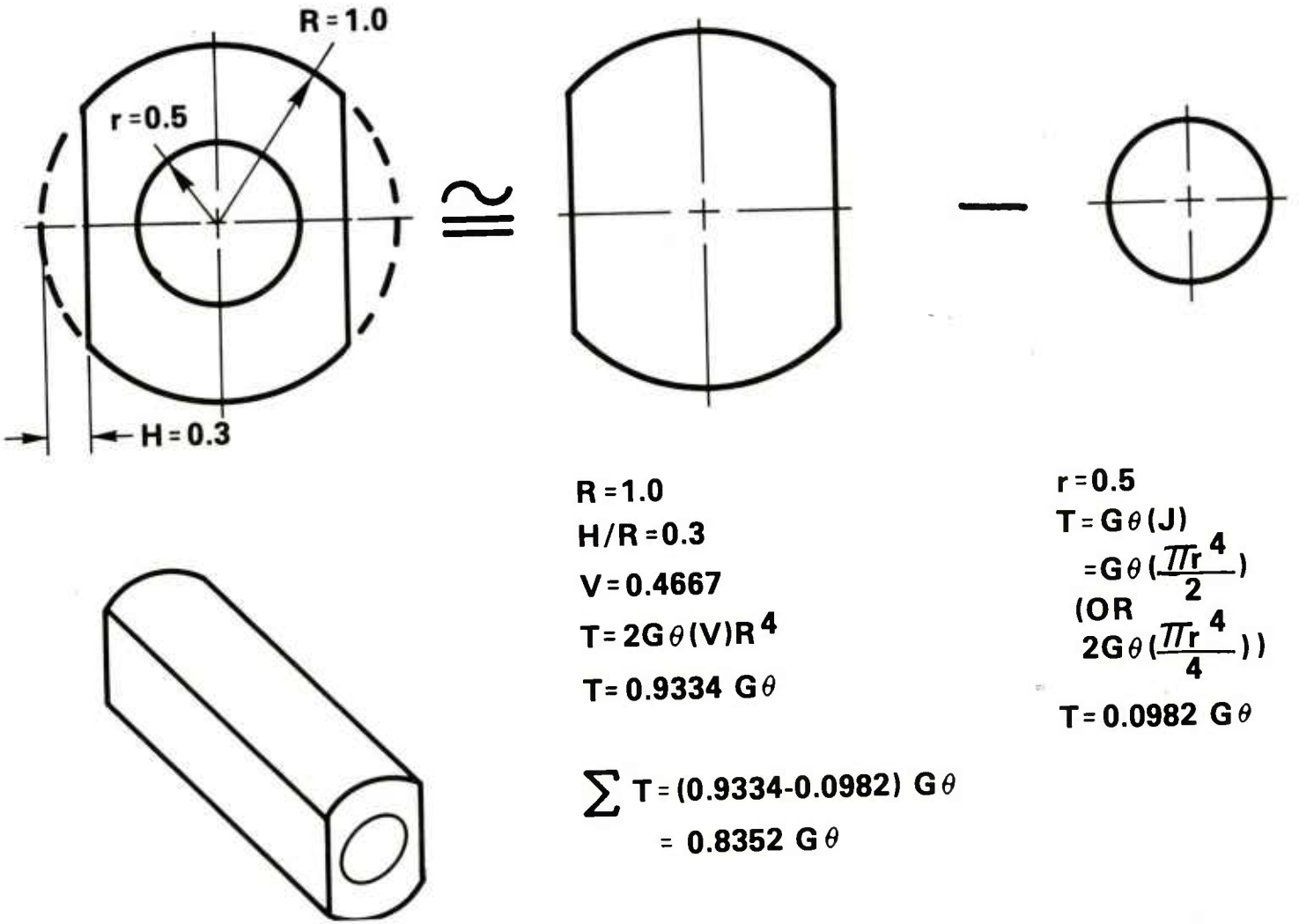

Figure 27. Milled shaft with central hole.

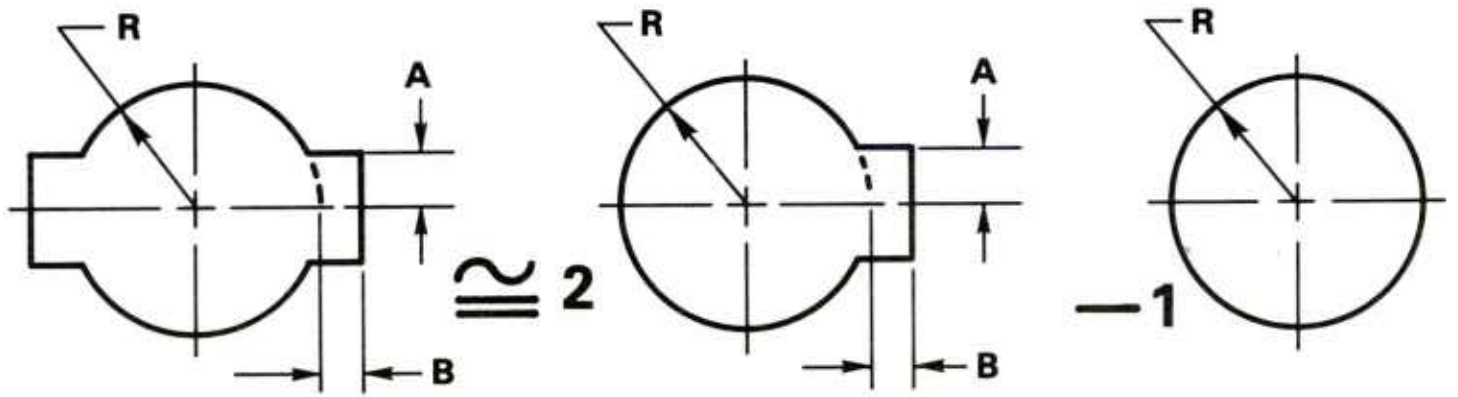

$R = 1.0, A = B = 0.4, \therefore A/B = 1.0, B/R = 0.1$

$V = 0.9595$	$V = 0.8712$	$V = \pi/4 = 0.7854$

$$VR^4 = 0.9595(1)^4 \stackrel{?}{=} \sum VR^4 = 2(0.8712)(1)^4 - 0.7854(1)^4$$

$$0.9595 = 1.7424 - 0.7854$$

$$= 0.9570$$

$$\text{VARIATION} = (0.9595 - 0.9570)/0.9595 = 0.0025/0.9595$$

$$= 0.26\%$$

Figure 28. Superposition for two spline shaft.

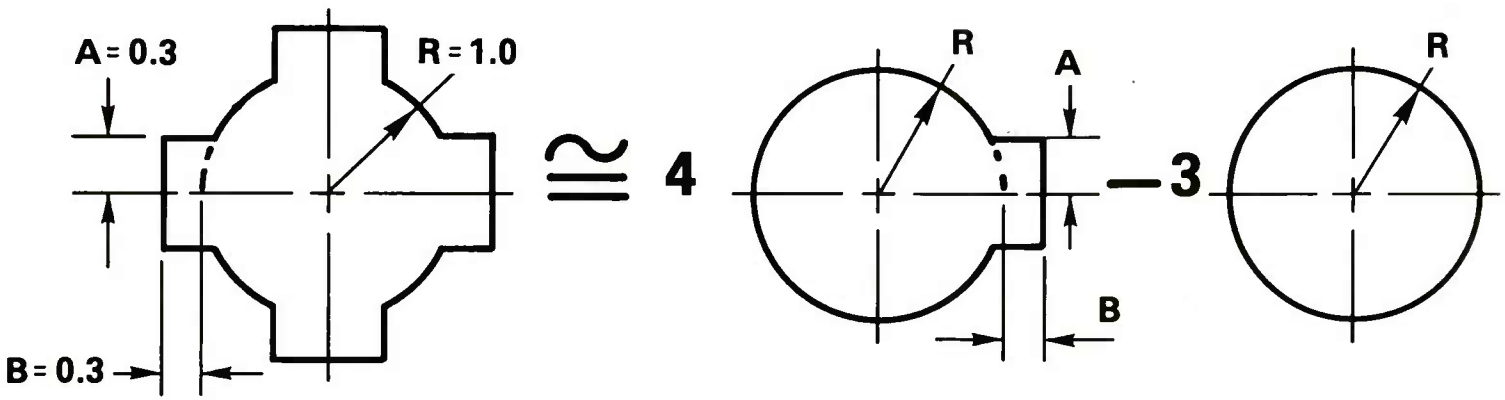

V = 0.9519	V = 0.8253	V = 0.7854

$$VR^4 = 0.9519\,(1)^4 \stackrel{?}{=} 4.(0.8253)\,(1)^4 - 3\,(0.7854)\,(1)^4$$

$$0.9519 = 3.3012 - 2.3562$$

$$0.9519 = 0.945 \quad \text{a 0.72\% VARIATION}$$

Figure 29. Superposition A for four spline shaft.

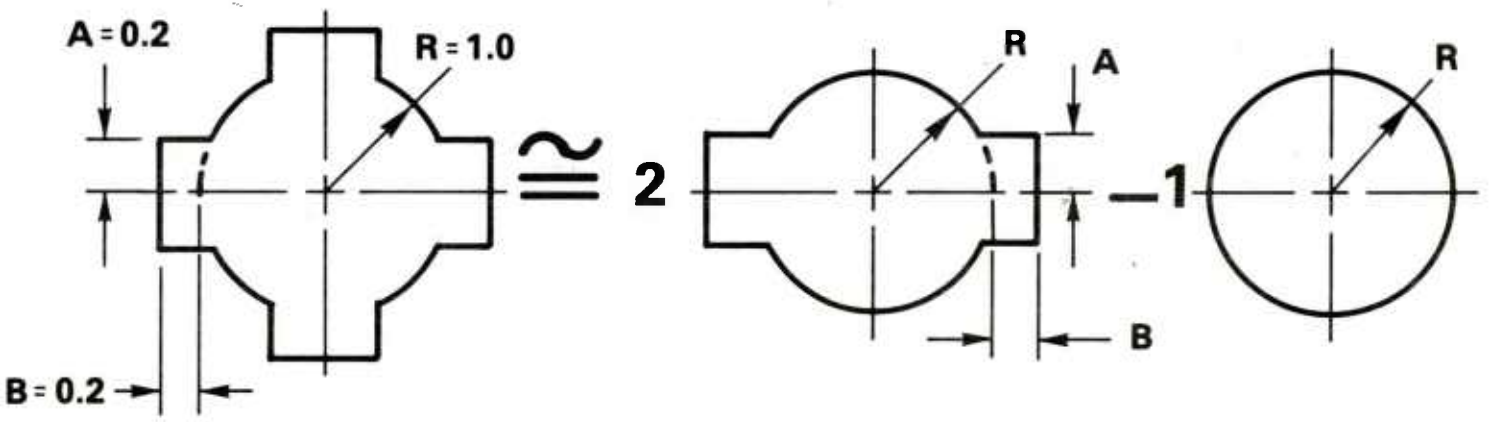

V = 0.8467		V = 0.8152		V = 0.7854
$VR^4 = 0.8467(1)^4$	$\stackrel{?}{=}$	$2(0.8152)(1)^4$	–	$(0.7854)(1)^4$
0.8467	=	1.6304-0.7854		
0.8467	=	0.845,a 0.2% VARIATION		

Figure 30. Superposition B for four spline shaft.

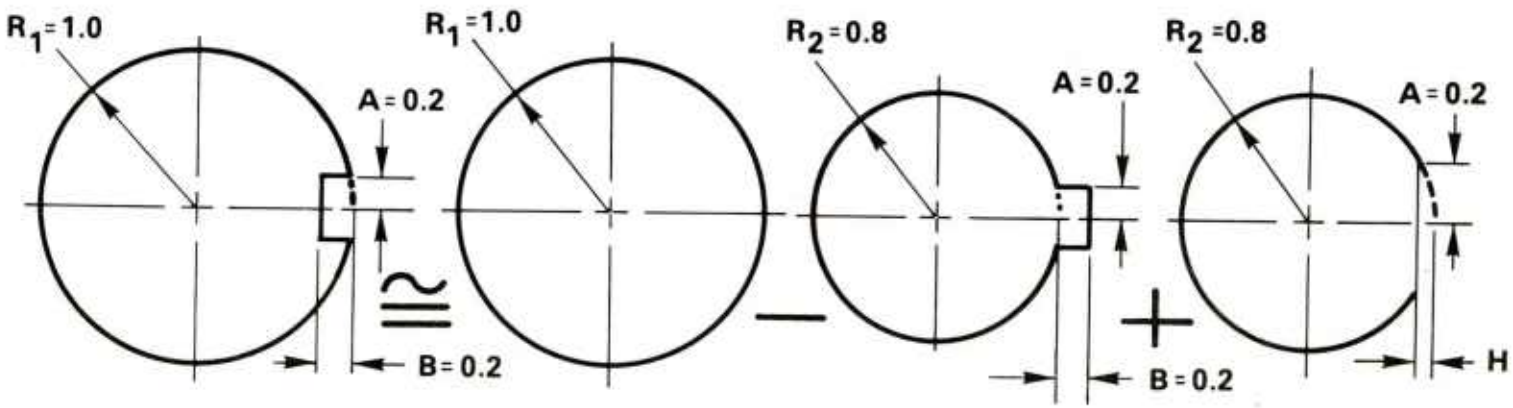

A/B = 1.0 B/R = 0.2 V = 0.7125 VR^4 = 0.7125	$V = \pi/4\ R^4$ = 0.7854 VR^4 = 0.7854	A/B = 1.0 B/R = 0.25 V = 0.8125 $VR^4 = 0.8125(0.8)^4$ = 0.3328	$H = R - \sqrt{R^2 - A^2}$ H = 0.0254 H/R = 0.0318 V = 0.7807 $VR^4 = 0.7807(0.8)^4$ = 0.3198

$0.7125 \stackrel{?}{=} \sum VR^4 = 0.7854 - 0.3328 + 0.3198$

$0.7125 = 0.7724$

VARIATION = (0.7724-0.7125)/0.7125 = 0.0599/0.7125

= 8.4%

Figure 31. Superposition for single keyway shaft.

BIBLIOGRAPHY

1. F. S. Shaw, "The Torsion of Solid and Hollow Prisms in the Elastic and Plastic Range by Relaxation Methods," Australian Council for Aeronautics, Report ACA-11, November 1944.

2. F. S. Shaw, An Introduction to Relaxation Methods, Dover Publications, Inc., Melbourne, Australia, 1953.

3. D. N. deG. Allen, Relaxation Methods, McGraw-Hill Book Company, Inc., New York, 1954.

4. D. H. Pletta and F. J. Maher, "The Torsional Properties of Round-Edged Flat Bars," Bulletin of the Virginia Polytechnic Institute, Vol XXXV, No. 7, Engineering Experiment Station Series No. 50, Blacksburg, Virginia, March 1942.

5. W. Ker Wilson, Practical Solution of Torsional Vibration Problems, Volume 1, 3rd Edition, John Wiley & Sons, Inc., New York, 1956.

6. R. I. Isakower and R. E. Barnas, "The Book of CLYDE - With a Torque-ing Chapter," U.S. Army ARRADCOM Users Manual MISD UM 77-3, Dover, NJ, October 1977.

7. R. I. Isakower and R. E. Barnas, "Torsional Stresses in Slotted Shafts," Machine Design, Volume 49, No. 21, Penton/IPC, Cleveland, Ohio, September 1977.

APPENDIX A

MATHEMATICAL MODEL USED IN THE CLYDE COMPUTER PROGRAM

As the term implies, boundary value problems are those for which conditions are known at the boundaries. These conditions may be the value of the problem variable itself (temperature, for example), the normal gradient or variable slope, or higher derivatives of the problem variable. For some problems, mixed boundary conditions may have to be specified: different conditions at different parts of the boundary. CLYDE solves those problems for which the problem variable itself is known at the boundary.

Given sets of equally spaced arguments and corresponding tables of function values, the finite difference analyst can employ forward, central, and backward difference operators. CLYDE is based upon central difference operators which approximate each differential operator in the equation.

The problem domain is overlaid with an appropriately selected grid. There are many shapes (and sizes) of overlaying Cartesian and polar coordinate grids:

rectangular
square
equilateral-triangular
equilangular-hexagonal
oblique

Throughout the area of the problem, CLYDE uses a constant-size square grid for which the percentage errors are of the order of the grid size squared (h^2). This grid (or net) consists of parallel vertical lines spaced h units apart, and parallel horizontal lines, also spaced h units apart, which blanket the problem area from left-to-right and bottom-to-top.

The intersection of the grid lines with the boundaries of the domain are called boundary nodes. The intersections of the grid lines with each other within the problem domain are called inner domain nodes. It is at these inner domain nodes that the finite difference approximations are

applied. The approximation of the partial differential equation with the proper finite difference operators replaces the PDE with a set of subsidiary linear algebraic equations, one at each inner domain node. In practical applications, the method must be capable of solving problems whose boundaries may be curved. In such cases, boundary nodes are not all exactly h units away from an inner node, as is the case between adjacent inner nodes. The finite difference approximation of the harmonic operator at each inner node involves not only the variable value at that node and at the four surrounding nodes (above, below, left, and right), but also the distance between these four surrounding nodes and the inner node. At the boundaries, these distances vary unpredictably. Compensation for the variation must be included in the finite difference solution. CLYDE represents the problem variable by a second-degree polynomial in two variables, and employs a generalized irregular "star" in all directions for each inner node. In practice, one should avoid a grid so coarse that more than two arms of the star are irregular (or less than h units in length). The generalized star permits, and automatically compensates for, a variation in length of any of the four arms radiating from a node. For no variation in any arm, the algorithm reduces exactly to the standard harmonic "computation stencil."

At each inner domain node, a finite difference approximation to the governing partial differential equation (PDE) is generated by CLYDE. The resulting set of linear algebraic equations is solved simultaneously by the program for the unknown problem variable (temperature, voltage, stress function, etc.) at each node in the overlaying finite difference grid. A graphics version of the program also generates, and displays on the CRT screen, iso-value contour maps for any desired values of the variable. This way, a more meaningful picture of the solution in the form of temperature distributions, constant voltage lines, stress concentration graphs, or even contour lines of different values of deformation and bending moment in structural problems, is made available to the engineer.

The user may also specify a finer grid spacing to increase resolution in critical regions of the problem, modify the scale of the display, change the boundary of the problem or redraw it completely, and change boundary conditions and coefficients--all at the face of the screen. It is also possible to request CLYDE to pass a plane through the two dimenslonal picture displayed on the screen. This plane is perpendicular to the screen and appears as a straight line. CLYDE will generate a new display showing a cross section (or elevation) view from the edge or

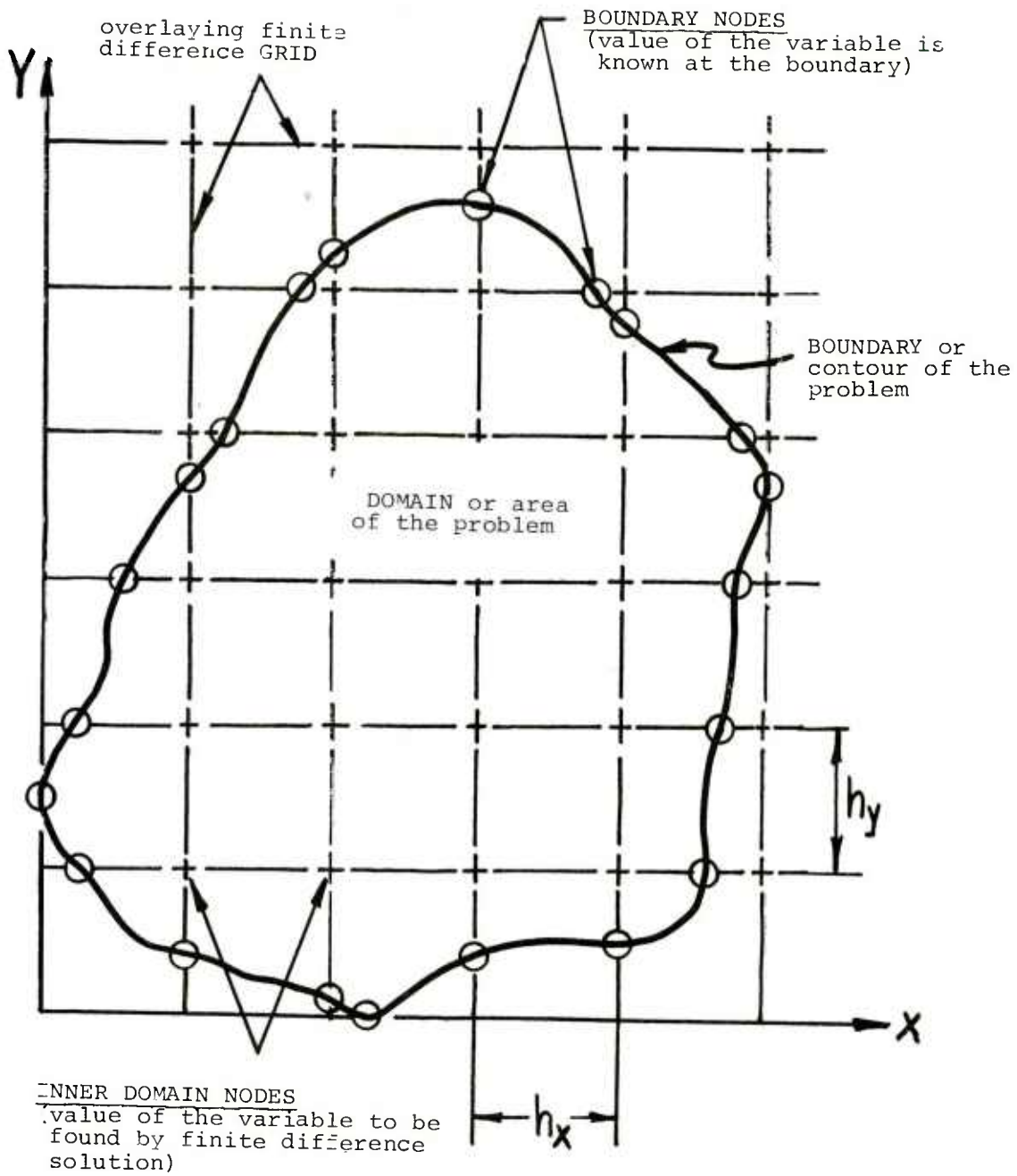

Figure A-1. Finite difference grid.

side. In this manner the variation or plot of the solved variable along that line is displayed on the screen. If the problem geometry is symmetrical, the designer does not have to display and work with the entire picture of the problem, he need only work with the "repeating section." In essence, the graphics user may examine the problem solution at will and redesign the problem (contour, boundary conditions, equation coefficients, etc.) at the screen resolving the "new design" problem.

Consider the general expression:

$$\nabla^2 f = A \frac{\partial^2 f}{\partial \eta^2} + B \frac{\partial^2 f}{\partial \xi^2} + \frac{c}{\lambda} \frac{\partial f}{\partial \lambda} = D \qquad \text{Eq (1)}$$

in the η, ξ, λ coordinate system, where A, B, C, D are arbitrary constants.

When $C = 0$, $\nabla^2 f$ reduces to a two-coordinate system, in X and Y, for example:

$$\nabla^2 f = A \frac{\partial^2 f}{\partial x^2} + B \frac{\partial^2 f}{\partial y^2} = D \qquad \text{Eq (2)}$$

Using central differences, the finite difference approximations to the partial differential operators of function f at representative node O are:

$$\frac{\partial f}{\partial x} = \frac{1}{2h_x} (f_1 - f_3), \quad \frac{\partial f}{\partial y} = \frac{1}{2h_y} (f_2 - f_4)$$

$$\frac{\partial^2 f}{\partial x^2} = \frac{1}{h_x^2} (f_1 - 2 f_0 + f_3)$$

$$\frac{\partial^2 f}{\partial y^2} = \frac{1}{h_y^2} (f_2 - 2 f_0 + f_4) \qquad \text{Eq (3)}$$

for a square grid, $h_x = h_y = h$ and the harmonic operator $\nabla^2 f$ becomes:

$$h^2 \nabla^2 f_0 = [A (f_1 + f_3) + B (f_2 + f_4) - (A+B) 2f_0] = h^2 D \qquad \text{Eq (4)}$$

see figure A-4.

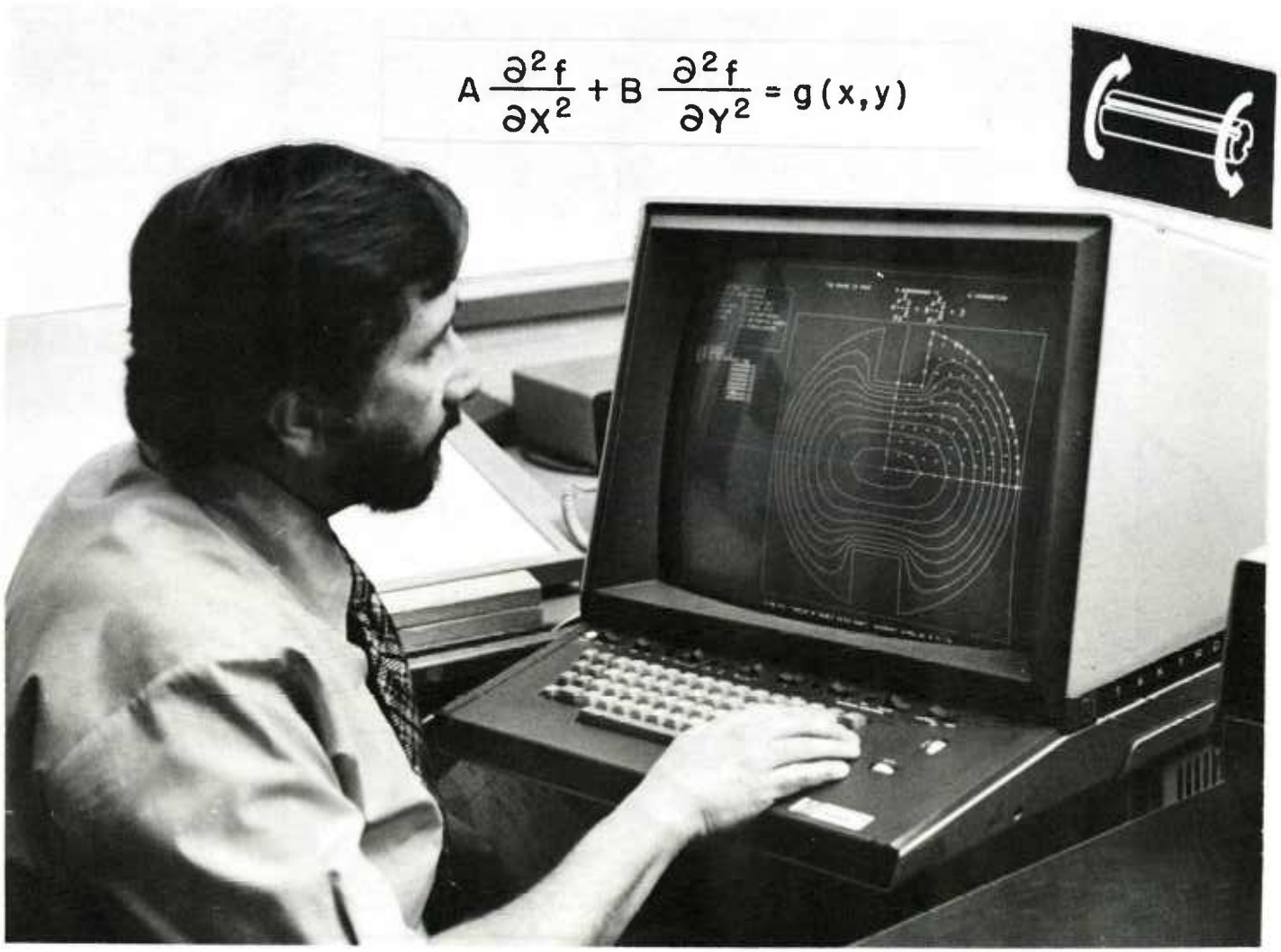

Figure A-2. Contour map of stress function for two keyway shaft.

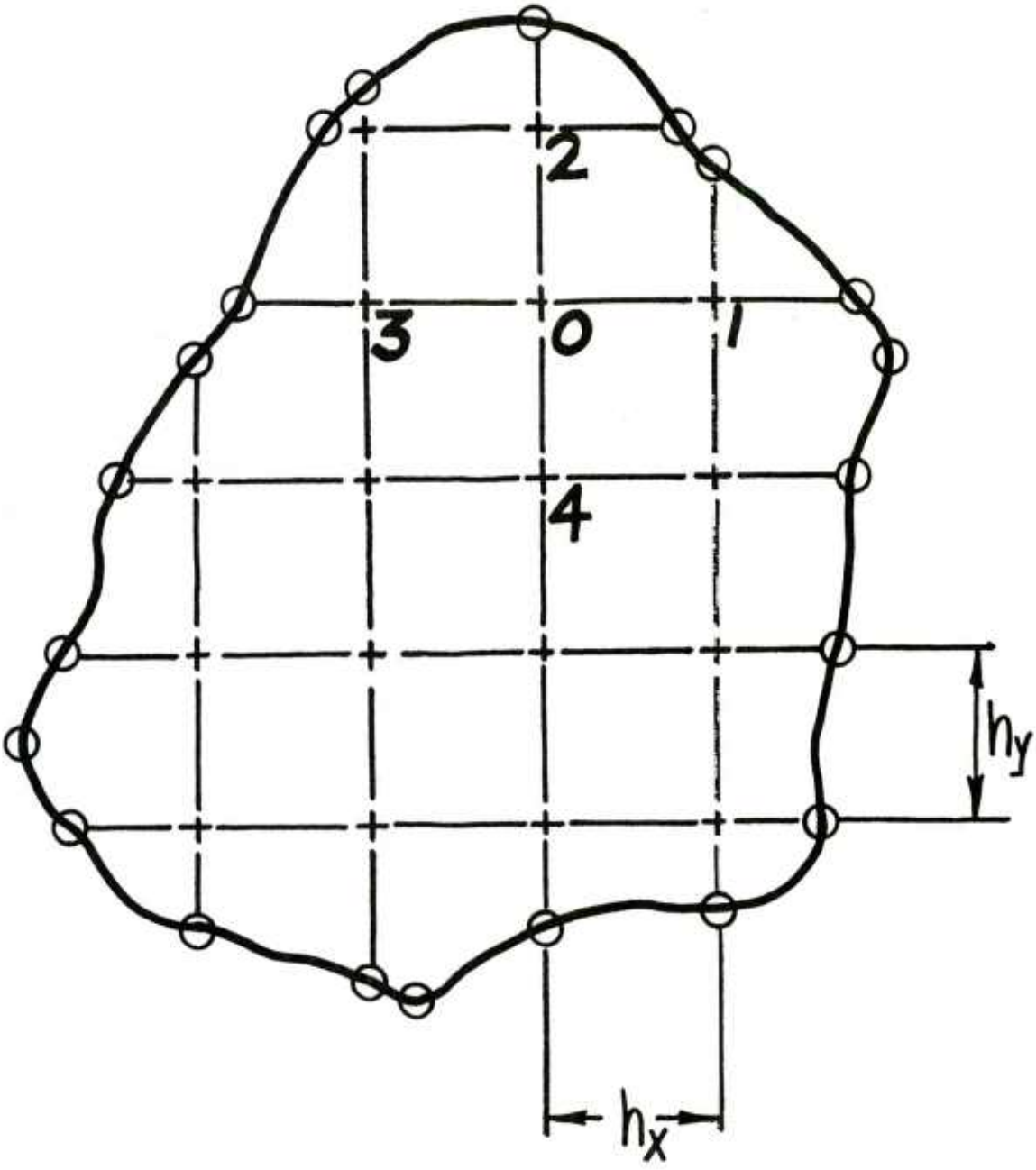

Figure A-3. Inner domain nodes.

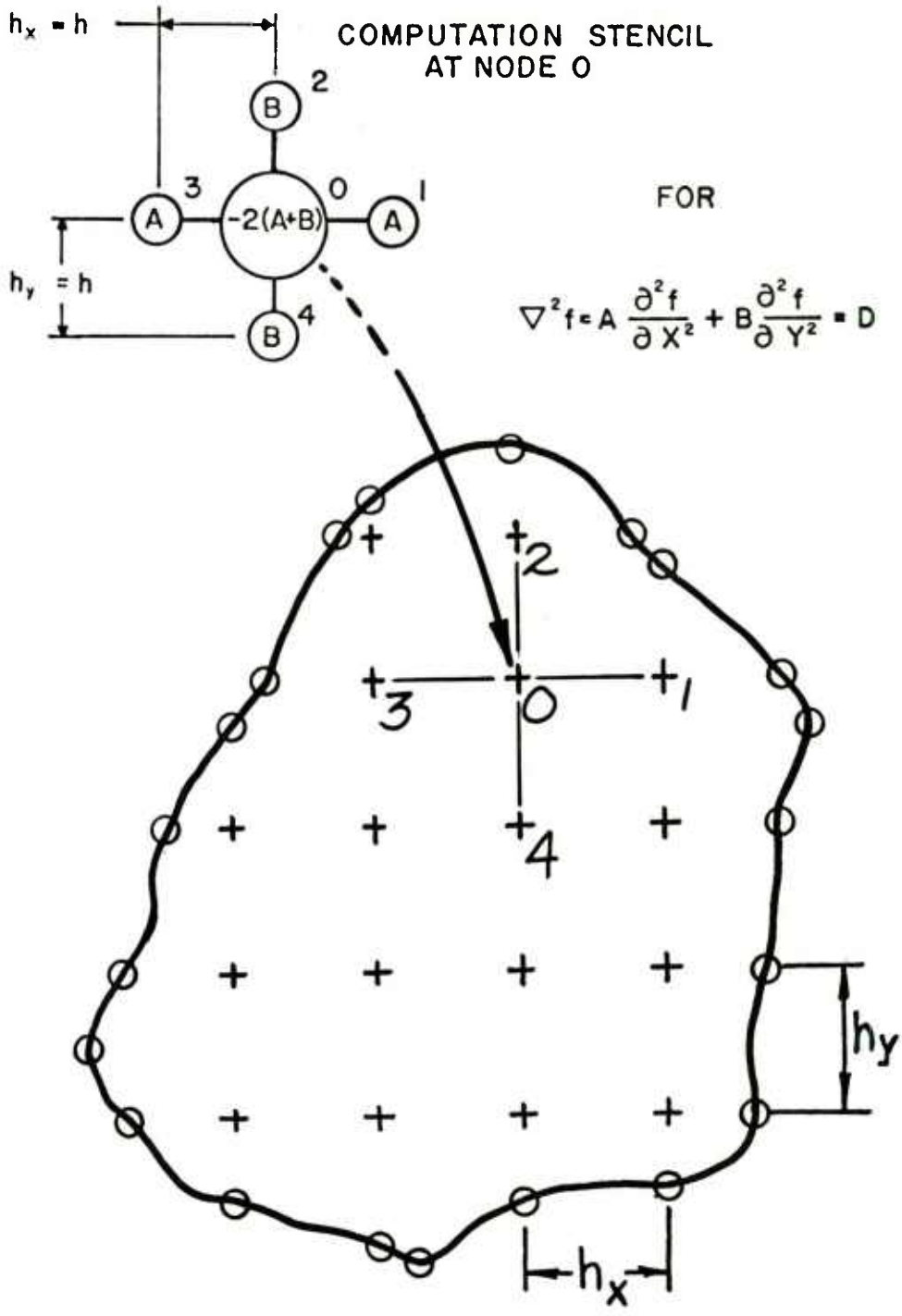

Figure A-4. Harmonic operator for square star in X-Y grid.

This finite difference equation at node zero involves the unknown variable at node zero (f_0) plus the unknown value of the variable at the four surrounding nodes (f_1, f_2, f_3, f_4), plus the grid spacing (h). The five nodes involved form a four-arm star with node zero at the center. This algebraic (or difference) equation could be conveniently visualized as a four-arm computation stencil made up of five "balloons" connected in a four-arm star pattern and overlayed on the grid nodes. The value within each balloon is the coefficient by which the variable (f) at that node is multiplied to make up the algebraic approximation equation.

The numerical treatment of an irregular star ($h_1 \neq h_2 \neq h_3 \neq h_4$) represents the function f near the representative node O by a second-degree polynomial in X and Y:

$$f(X,Y) = f_0 + a_1X + a_2Y + a_3X^2 + a_4Y^2 + a_5XY \qquad \text{Eq (5)}$$

Evaluating this polynomial at the neighboring nodes (1, 2, 3, 4) produces the following set of equations:

$$f_1 = f_0 + a_1h_1 + a_3h_1^2$$

$$f_2 = f_0 + a_2h_2 + a_4h_2^2$$

$$f_3 = f_0 - a_1h_3 + a_3h_3^2$$

$$f_4 = f_0 - a_2h_4 + a_4h_4^2 \qquad \text{Eq (6)}$$

which are then solved for a_3 and a_4 which are necessary to satisfy the harmonic operator $\nabla^2 f$, since:

$$\frac{\partial f}{\partial x} = a_1 + 2a_3X + a_5Y, \quad \frac{\partial^2 f}{\partial x^2} = 2a_3$$

$$\frac{\partial f}{\partial y} = a_2 + 2a_4Y + a_5X, \quad \frac{\partial^2 f}{\partial y^2} = 2a_4 \qquad \text{Eq (7)}$$

and

$$\nabla^2 f = A\,(2a_3) + B\,(2a_4) \qquad \text{Eq (8)}$$

Performing the necessary algebraic operations, substituting results, collecting terms, and using the following ratios:

$$b_1 = \frac{h_1}{h} \qquad b_2 = \frac{h_2}{h}$$

$$b_3 = \frac{h_3}{h} \qquad b_4 = \frac{h_4}{h} \qquad \text{Eq (9)}$$

The harmonic operator becomes:

$$h^2 \nabla^2 f_0 = \left[\frac{2A}{b_1 (b_1+b_3)} f_1 + \frac{2B}{b_2 (b_2+b_4)} f_2 + \right.$$

$$+ \frac{2A}{b_3 (b_1+b_3)} f_3 + \frac{2B}{b_4 (b_2+b_4)} f_4 +$$

$$\left. - \left(\frac{2A}{b_1 b_2} + \frac{2B}{b_2 b_4} \right) f_0 \right] = h^2 D \qquad \text{Eq (10)}$$

See figure A-5.

When $C \neq 0$, $\nabla^2 f$ can be applied to an axisymmetric cylindrical co-ordinate system, in R and Z, for example:

$$\nabla^2 f = A \frac{\partial^2 f}{\partial Z^2} + B \frac{\partial^2 f}{\partial R^2} + \frac{C}{R} \frac{\partial f}{\partial R} = D \qquad \text{Eq (11)}$$

For a regular star, the harmonic operator becomes (in a similar manner to equation 4):

$$h^2 \nabla^2 f_0 = \left[A (f_1 + f_3) + B (f_2 + f_4) + \frac{Ch}{2R_0} (f_2 - f_4) \right.$$

$$\left. - (A + B) 2 f_0 \right] = h^2 D \qquad \text{Eq (12)}$$

See figure A-6.

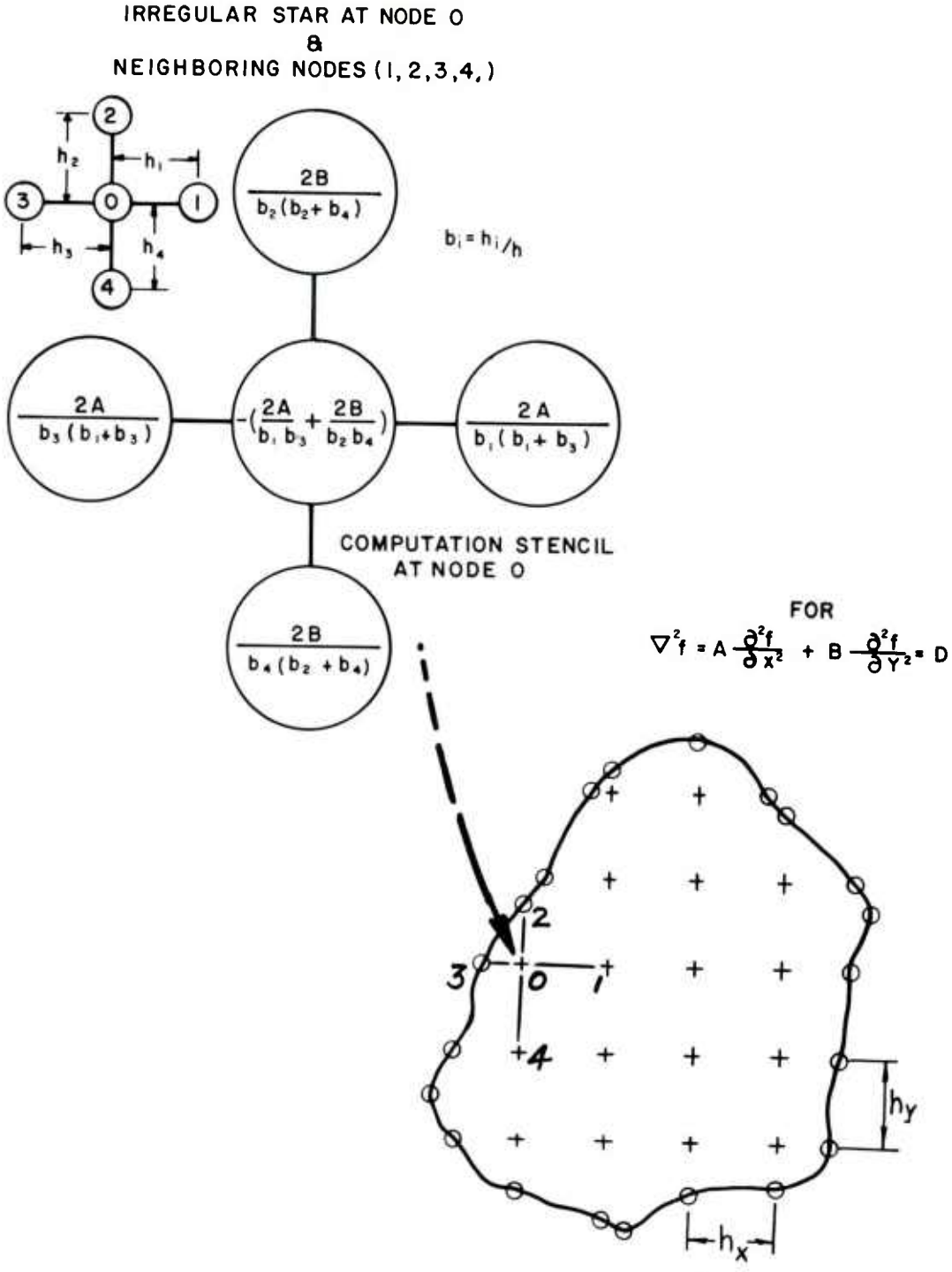

Figure A-5. Harmonic operator for irregular star in X-Y grid.

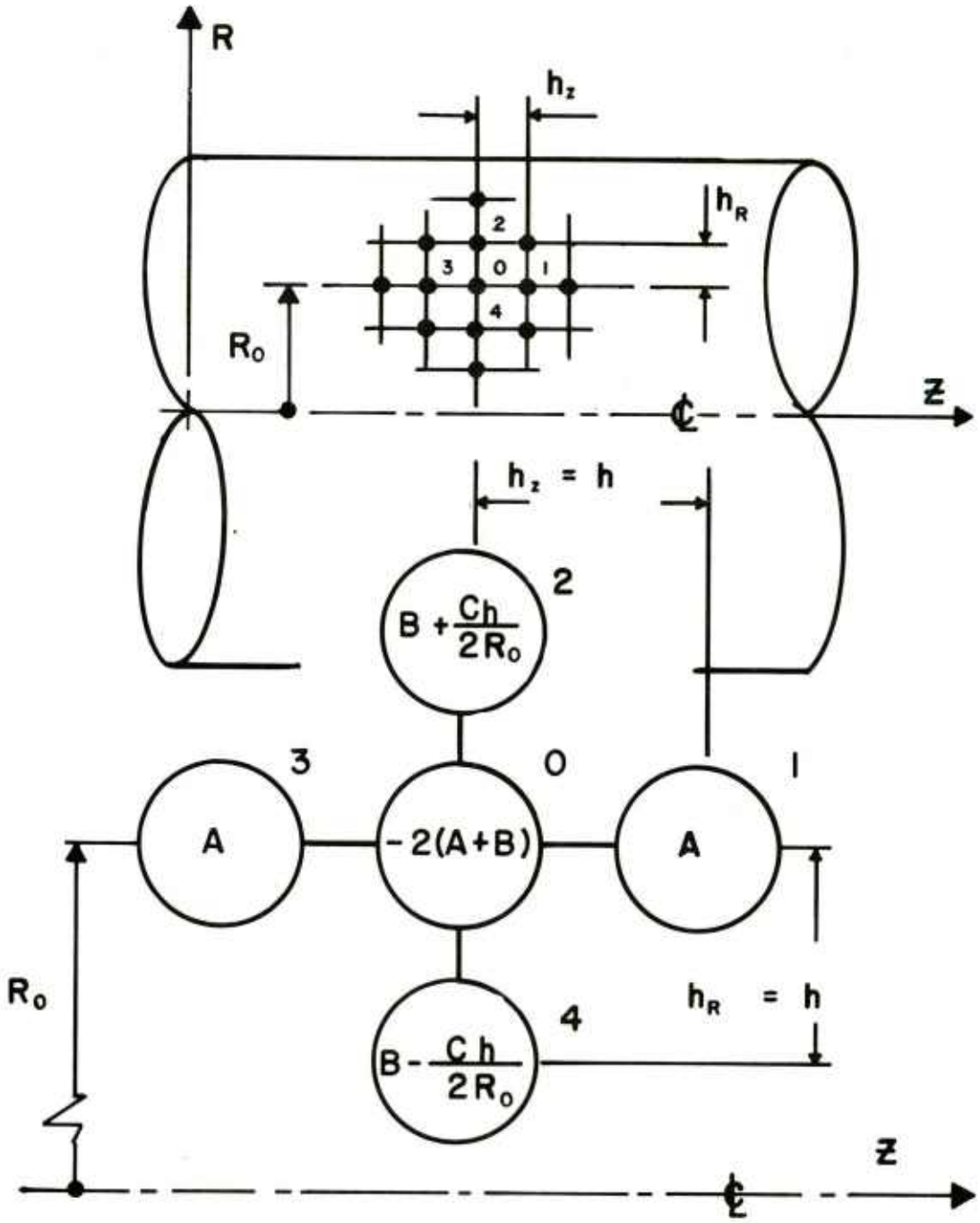

Figure A-6. Harmonic operator for square star for R-Z grid.

For an irregular star ($h_1 \neq h_2 \neq h_3 \neq h_4$), the harmonic operator becomes (in a manner similar to equation 10):

$$h^2 \nabla^2 f_0 = \left[\frac{2A}{b_1 (b_1+b_3)} f_1 + \frac{2B}{b_2 (b_2+b_4)} f_2 + \right.$$

$$+ \frac{2A}{b_3 (b_1+b_3)} f_3 + \frac{2B}{b_4 (b_2+b_4)} f_4 +$$

$$+ \frac{Ch}{R_0} \left\{ \frac{b_4}{b_2 (b_2+b_4)} f_2 - \frac{b_2}{b_4 (b_2+b_4)} f_4 \right\} +$$

$$\left. - \left\{ \frac{2A}{b_1 b_3} + \frac{2B}{b_2 b_4} - \frac{Ch}{R_0} \left(\frac{b_2-b_4}{b_2 b_4} \right) \right\} f_0 \right]$$

$$= h^2 D \qquad \text{Eq (13)}$$

See figure A-7.

Equations 10 and 13 are employed in the programmed solutions for Cartesian and cylindrical coordinates, respectively.

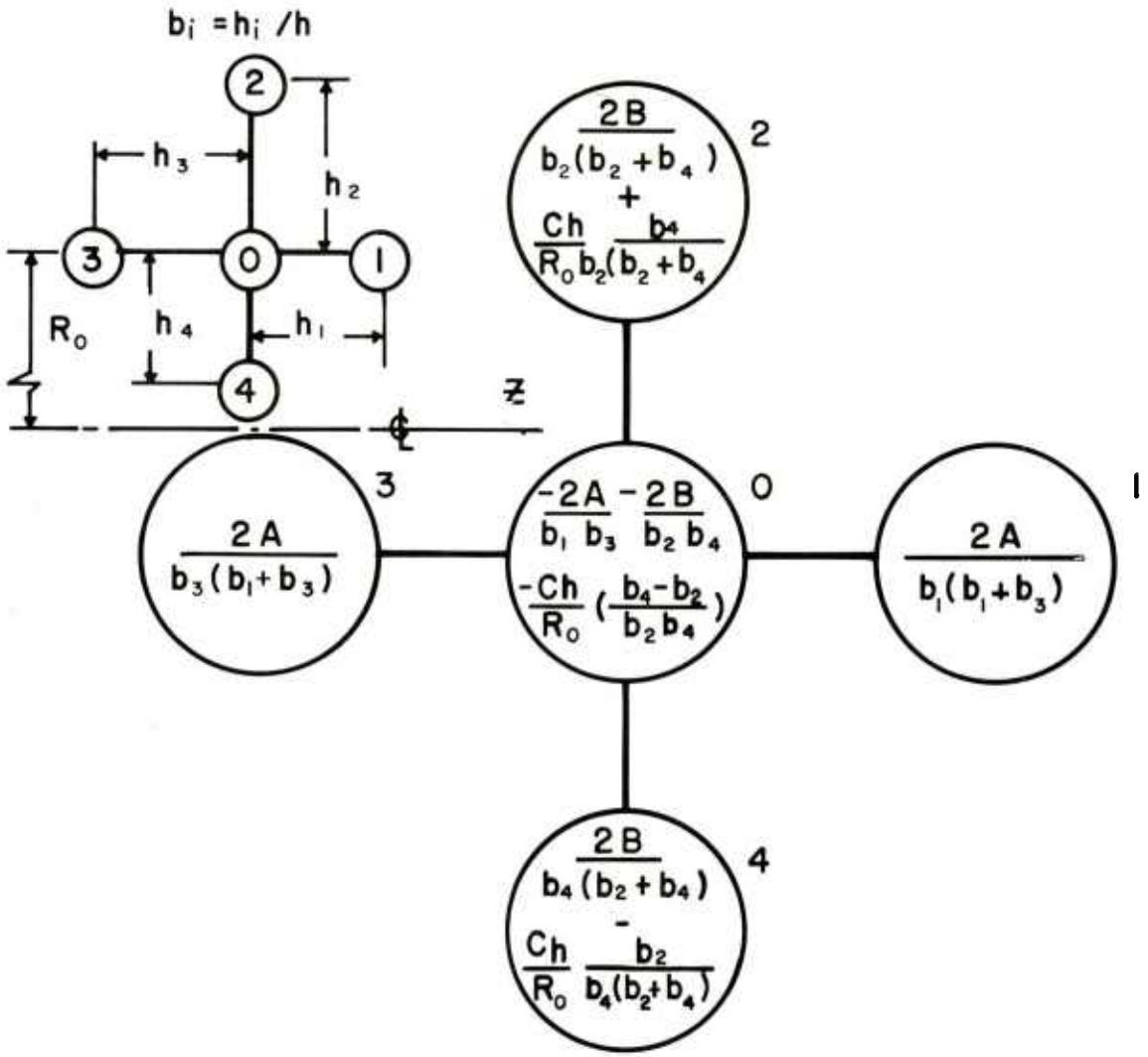

Figure A-7. Harmonic operator for irregular star in R-Z grid.

APPENDIX B

EXTENSION OF MODEL TO HOLLOW SHAFTS

This would appear to be a simple matter of solving the governing PDE over a multiply-connected boundary, were it not for the uncertainty concerning boundary conditions. The actual value of the problem variable at the boundary was not important in the torsion application, only the difference in the problem variable at various points mattered. The problem variable at the boundary could be assumed to have any value, as long as there was only one boundary. With two or more boundaries the solution calls for a different approach.

The stress function is obtained as the superposition[1] of two solutions, one of which is adjusted by a factor (k). This is the planned programmed solution to shafts with a hole. The hole may be of any shape, size, and location. The two solutions, to be combined, are shown in figure B-1: equations and boundary conditions. This capability already exists in CLYDE. The solution for k will be added, and then the final superposition of results. Once the contour integrals are taken around the inner boundary of area A_B, the only unknown, k, may be readily obtained. The contour integral, which need not be evaluated around the actual boundary, may be taken around any contour that encloses that boundary, and includes none other (for example, see shaded area A_B) in figure B-1.

[1] F. S. Shaw, The Torsion of Solid and Hollow Prisms in the Elastic and Plastic Range by Relaxation Methods, Australian Council for Aeronautics, Report ACA-11, November 1944, pp 8, 11, 23.

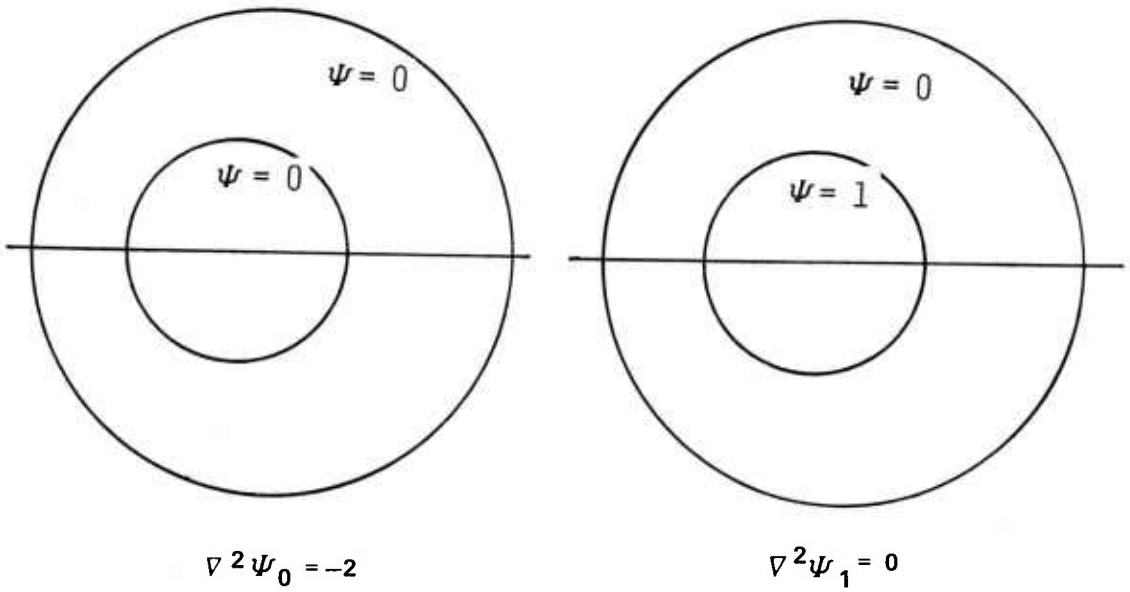

$\nabla^2 \Psi_0 = -2$ $\qquad$ $\nabla^2 \Psi_1 = 0$

$$\Psi = \Psi_0 + k\,\Psi_1$$

$$-2A_B = \oint \frac{\partial \Psi_0}{\partial \nu}\, ds + k \oint \frac{\partial \Psi_1}{\partial \nu}\, ds$$

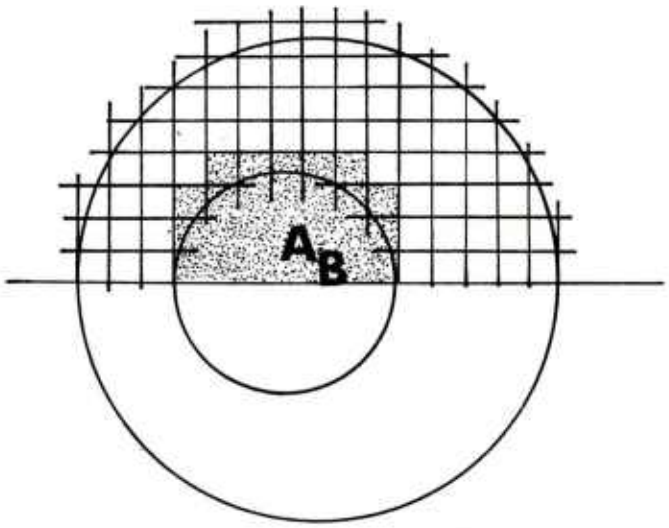

Figure B-1. Mathematical approach to hollow shaft problem.

DISTRIBUTION LIST

Commander
U.S. Army Armament Research
and Development Command
ATTN: DRDAR-TD
DRDAR-LCU-T, Mr. J. Dubin
Mr. A. Berman
Mr. J. Pearson
DRDAR-LCF-A, Mr. B. Schulman
Dr. F. Tepper
Mr. L. Wisse
DRDAR-LCA, Mr. L. Rosendorf
Mr. C. Larson
Mr. B. Knutelski
DRDAR-SCS, Mr. H. Cohen
Mr. E. Jarosjewski
Mr. R. Kwatnoski
Mr. J. Bevelock
DRDAR-SCF, Mr. A. Tese
DRDAR-MS
DRDAR-MSA, Mr. R. Isakower (5)
Mr. R. Barnas
Mr. J. Sierodzinski
DRDAR-MSM, Mr. B. Barnett (5)
DRDAR-MST, Mr. I. Rucker
DRDAR-MSH, Mr. A. G. Edwards
DRDAR-TSS (5)
Dover, NJ 07801

Commander
U.S. Army Armament Research
and Development Command
ATTN: DRDAR-LCB, Mr. J. Pascale
Watervliet, NY 12189

Commander
U.S. Army Armament Research
and Development Command
ATTN: DRDAR-BLB, Dr. S. Taylor
DRDAR-MSG, Mr. M. Romanelli
Aberdeen Proving Ground, MD 21005

Commander
U.S. Army Armament Research
and Development Command
ATTN: DRDAR-MSE, Mr. S. Goldberg
Aberdeen Proving Ground, MD 21010

Commander
Brook Army Medical Center
ATTN: SP4 Lillian Ishibashi
Cardiovascular Lab Data Analysis
Fort Sam Houston, TX 78234

Commander
U.S. Army Missile Research
and Development Command
ATTN: DRDMI-HRD, Mr. Siegfried H. Lehnigk
Redstone Arsenal, AL 35809

Commander
U.S. Army Research and Technology Laboratories
ATTN: DAVDL-EU-TSC
Fort Eustis, VA 23604

Commander
U.S. Army Tank-Automotive Research
and Development Command
ATTN: DRDTA-UL, Technical Library
Warren, MI 48090

Commander
U.S. Navy Surface Weapons Center
ATTN: NSWC, Mr. W. P. Warner
Technical Library
Dahlgren, VA 22448

Commander
U.S. Navy Surface Weapons Center
White Oak Laboratory
ATTN: NOL, Mr. J. Franklin
Technical Library
Silver Spring, MD 20910

Commander
U.S. Naval Ship Research and
Development Center
ATTN: NSRDC, Mr. P. Matula
Mr. J. McKey
Technical Library
Bethesda, MD 20034

Commanding Officer
NASA Langley Research Center
ATTN: NLRC, Dr. Fulton
Technical Library
Hampton, VA 22065

Martin Marietta Aerospace
Denver Division
ATTN: Mr. Michael M. Davis
Mass Properties Engineering
PO Box 179
Denver, CO 80201

Sperry Vickers
North American Group
ATTN: Mr. Frank Rosett
1401 Crooks Road
Troy, MI 48084

The Bendix Corporation
ATTN: Mr. David F. Theilen
Department 744, MC45
PO Box 1159
Kansas City, MO 64141

College of the City of New York
Technology Department
ATTN: Professor Sandor Halasz, Chairman
Steinman Hall 207-14
Convent Avenue and 138th Street
New York, NY 10031

Professor Theodore Baumeister
Yonges Island, SC 29494

College of the City of New York
Mechanical Engineering Department
ATTN: Professor Eugene A. Avallone
Convent Avenue & 138th Street
New York, NY 10031

E. I. duPont deNemours and Company
ATTN: Information Systems Dept,
Mr. Theodore Baumeister, III
Engineering Dept,
Dr. Joseph H. Faupel (2)
Wilmington, DE 19898

University of Wisconsin
ATTN: Dr. Warren C. Young (2)
537 Engineering Research Bldg
1500 Johnson Drive
Madison, WI 53706

Stanford University
ATTN: Dr. W. Flügge (2)
Applied Mechanical Engineering Dept
Stanford, CA 94305

Defense Documentation Center (12)
Cameron Station
Alexandria, VA 22314

Weapon System Concept Team/CSL
ATTN: DRDAR-ACW
Aberdeen Proving Ground, MD 21010

Technical Library
ATTN: DRDAR-CLJ-L
Aberdeen Proving Ground, MD 21010

Technical Library
ATTN: DRDAR-TSB-S
Aberdeen Proving Ground, MD 21005

Benet Weapons Laboratory
Technical Library
ATTN: DRDAR-LCB-TL
Watervliet, NY 12189

Commander
U.S. Army Armament Materiel
Readiness Command
ATTN: DRSAR-LEP-L
Rock Island, IL 61299

Director
U.S. Army TRADOC Systems
Analysis Activity
ATTN: ATAA-SL (Tech Library)
White Sands Missile Range, NM 88002

U.S. Army Materiel Systems
Analysis Activity
ATTN: DRXSY-MP
Aberdeen Proving Ground, MD 21005